



NTNU – Trondheim
Norwegian University of
Science and Technology

Photon Activity from Partial Discharges in Liquid Dielectrics

Experimental test setup and measurements

Jan Eikeset

Master of Energy and Environmental Engineering

Submission date: June 2014

Supervisor: Arne Nysveen, ELKRAFT

Co-supervisor: Frank Mauseth, ELKRAFT

Norwegian University of Science and Technology
Department of Electric Power Engineering

Preface

This thesis builds upon a previous specialization project, conducted during the second half of 2013, at NTNU Trondheim.

I would like to thank my supervisors Arne Nysveen and Frank Mauseth, for their help and guidance. I would also sincerely thank Lars Lundgaard at SINTEF Energi AS and Dag Linhjell at NTNU for their help during the experimental work, and their enthusiastic guidance regarding any general queries. Thanks to Bård Almås at NTNU for helping me find all the needed parts in the laboratory.

Trondheim June 2014

Jan Eikeset

Abstract

New subsea processing plants are planned to operate at large depths, down to 5000 meters. Power electronic converters are a crucial part of the plants hardware. In order for the converters to operate at such deep depths, they are placed inside steel vessels. Current utilized technology have atmospheric conditions inside the steel vessels. The wall thickness may be as large as $\approx 10\text{cm}$, in order to handle the large external pressure. This solution is expensive and introduce other complications for the operation of the converters. A new design consist of filling the steel vessels with pressure compensated dielectric liquids, known as *Pressure Tolerant Power Electronics*.

The high power rating for some parts of the converters can introduce high electrical field stress in some locations. This field stress may initiate partial discharges inside the converter vessels. This is an unwanted phenomenon, since partial discharges may damage and deteriorate the liquid insulation and power electronic components. In worst case, the partial discharges can develop into complete electrical breakdowns. Routine tests of partial discharge activity is therefore crucial inside the converter vessels, in order to monitor the condition of the converter. However, it can be problematic separating actual partial discharges from other noise sources in system, such as stray capacitance and fast switching. Hence, precise electrical partial discharge measurement may be difficult to conduct.

This thesis study the correlation between light emission and the charge magnitude from partial discharges in different dielectric liquids. Light measurement is believed to be a capable method to monitor certain exposed fixed points inside the converter vessels. Most of the work is experimental, and consist of building a noise free, $<0.5\text{pC}$, resonance test circuit, with the ability to measure PD activity in dielectrical liquids both optically and electrically.

Partial discharges are initiated across a point-plane electrode configuration, inside a 1.6 litre test-cell. A *Hamamatsu R1635 Photo Multiplier Tube*, in combination with an oscilloscope is used to register photon activity in the partial discharges. *Power Diagnostix ICM System* is used to measure electrical partial discharge signals.

The experiments have revealed a correlation between emitted light and partial discharge magnitude for some dielectric liquids. Especially promising correlations are seen between the large and crucial partial discharges, $>0.5\text{nC}$. In addition, correlations between emitted light and partial discharge energy is registered. As for smaller partial discharges some cohesiveness seem to exists, but vary greatly for different dielectrical liquids. Further work about the subject is needed before the results can be practically useful. However, promising tendencies are observed.

Sammendrag

Nye undersjøiske prosesseringsanlegg er planlagt å bli montert på havdyp, ned til 5000 meter. Krafterelektroniske omformere er en viktig del av anleggene. Omformerne er plassert inni «ståltanker» for å klare å operere på havdypet. Dagens teknologi består av ståltanker med atmosfæriske forhold på innsiden av konstruksjonen. Stålveggene må være tjukke, opp til $\approx 10\text{cm}$, for å klare å takle det eksterne trykket fra vannet. Dette designet er dyrt, og kompliserer blant annet kjøling av omformeren. En ny type design går ut på å fylle omformertankene med trykksatt dielektrisk olje, kalt *Pressure Tolerant Power Electronics*.

Den store effektlasten krevd for deler av omformerne gjør at stor elektrisk feltstyrke kan oppstå på områder på/ved omformerne. Denne feltstyrken kan igangsette partielle utladninger inne i omformertankene. Slike utladninger er uønsket, der de kan forringe den elektriske isolasjonen og føre til slitasje på komponentene. I verste fall kan et fullstendig elektrisk overslag inntreffe, noe som er svært uheldig. Derfor er det ønskelig å kunne overvåke aktiviteten av partielle utladninger inne i omformertankene, slik at man kan kontrollere tilstanden til utstyret i bruk. Elektrisk måling av slike partielle utladninger kan være vanskelig å gjennomføre. Annen støy i kretsen, som utladning av parasittiske kondensatorer, kan ligne på strømsignalet fra partielle utladninger.

Denne masteroppgaven studerer sammenhengen mellom lysutsendelse og ladningsstørrelsen på partielle utladninger i forskjellige dielektriske væsker. Tanken er at lysmålinger kan overvåke spesielt utsatte områder for partielle utladninger inni omformertankene. Det meste av arbeidet i oppgaven er praktisk, og består i å bygge en støyfri målekrets, $>0,5\text{pC}$, som kan operere i resonans, og måle partielle utladninger i form av lys samt elektriske strømpulser.

Partielle utladninger er fremprovosert over et punkt-plate gap, plassert inne i en 1,6 l testcelle, fylt med dielektrisk olje. Et R1635 *Hamamtsu Photo Multiplier Tube* sammen med et oscilloskop er brukt til å registrere foton aktivitet i de partielle utladningene. *Power Diagnostix ICM System* er brukt til å måle de partielle utladningene elektrisk.

Forsøkene har vist at det er en viss sammenheng mellom lysutsendelse og størrelsen på partielle utladninger i noen dielektriske væsker. Spesielt lovende sammenheng er observert mellom store og viktige utladninger, $>0,5\text{nC}$. I tillegg er sammenheng mellom lysutsendelse og energimengde i de partielle utladningene undersøkt. Mer arbeid er nødvendig innenfor dette feltet før disse resultatene er praktisk anvendbare, men lovende tendenser er observert.

Abbreviations

- AC: Alternating Current
- DC: Direct Current
- HV: High Voltage, above 1000V
- HVAC: High Voltage Alternating Current
- PD: Partial Discharge
- PMT: Photo Multiplier Tube
- PTPE: Pressure Tolerant Power Electronics

Table of Content

Preface.....	i
Abstract	iii
Sammendrag	v
Abbreviations	vii
1. Introduction	1
1.1 Background	1
1.2 Problem Description	3
1.3 Limitations	3
2. Theory	4
2.1 Partial Discharge	4
2.1.1 PD Development in Liquids	4
2.2.2 PD Propagation and Streamer Phenomenon.....	6
2.2.3 Light Emission from PD Streamers.....	8
2.2.4 Additives effect on PD.....	8
2.2.5 PD as Stochastic Phenomenon	9
2.2 Point-Plane Geometry	9
2.3 Space Charges in the Liquid Dielectrics	11
2.4 Oil Light Emission.....	12
3. Method and Experimental Work	15
3.1 Laboratory Setup	15
3.1.1 Test Cell.....	16
3.1.2 Signal Generator and Power Amplifier	18
3.1.3 Power Diagnostix ICM System	18
3.1.4 Photo Multiplier Tube	19
3.1.5 RC-integrator and 2/4/6-preapmlifier	20
3.1.6 Oscilloscope	21
3.2 Resonance Circuit	21
3.3 Selection of Dielectric Liquids.....	22
3.3.1 Nytro 10XN.....	22
3.3.2 MIDEL7131	23
3.3.3 Galden HT200.....	23
3.3.4 EXXSOL D80	24

3.4 Test Procedure.....	24
3.5 Practical Considerations	25
4. Results.....	27
4.1 Circuit Resonance	27
4.1.1 Model and Simulations	27
4.1.2 Experimental Test Circuit Calculations	29
4.2 Electrical Field.....	32
4.3 PD Measurements	32
4.3.1 Nytro 10XN.....	34
4.3.2 MIDEL 7131	36
4.3.3 Galden HT200.....	39
4.3.4 EXXSOL D80.....	41
4.3.5 Combined PD Plot	41
5. Discussion.....	43
5.1 Test Circuit.....	43
5.1.1 Simulink Model	43
5.1.2 Test Circuit Behaviour.....	43
5.2 Partial Discharges	44
5.2.1 PD development.....	44
5.2.2 PD Charge Magnitude Measurements.....	45
5.2.3 Light Emission	46
5.2.4 Light Measurement vs. Electrical PD Pulse.....	46
5.3 Energy Comparison.....	47
6. Conclusion.....	49
7. Further Work.....	51
References.....	53
Appendix A	I
MATLAB Simulink Model	I
Appendix B	II
Transformer tests and calculations	II
T ₂ High Voltage Transformer 220:50 000	III
T ₁ isolating transformer 20/40/60:220	IV
Appendix C.....	V

Small negative PD data.....	V
Large positive PD data.....	VI

1. Introduction

1.1 Background

Subsea process plants are a relative new concept for the petroleum sector. Some plants are planned to operate at depths down to 3000-5000 meters. Installing pumps, refineries, pipes, power electronic converters, cables and other hardware on the seabed involves great challenges when it comes to component design. The hardware must be able to operate at deep depths involving high hydrostatic pressure. Seawater may deteriorate certain types of material, and fragile components must be kept isolated from the seawater. Installation processes are complicated, time consuming and expensive. Involving specialized vehicles, ROVs and personnel. It is therefore crucial that the subsea equipment has a long expected lifetime, with low demand for maintenance. Ultimately, all parts of the subsea plants should be self-monitoring, giving the operators sufficient information about the systems current condition.

Technology currently under testing, at e.g. "Ormen Lange", applies power converters installed inside atmospheric pressurised steel vessels. Thick steel walls, ≈ 100 mm, are needed to be able to handle the high pressure at deep-sea, up to 500 bars. Drawbacks to these subsea converters compared to conventional land based converters are:

- Increased weight, making it difficult to transport and install the converters.
- Increased cost, due to the amount of construction material needed for the vessel.
- Poor cooling of the converter, due to massive steel walls, preventing heat conduction.

SINTEF Energy Research and NTNU have an ongoing research project, sponsored by NFR and several industry partners, where the objective is to study and develop pressurized power converters, [1] [2] [3]. The concept is filling the vessels, containing the subsea power electronic converters, with dielectric liquids instead of atmospheric air. Liquid fills all gaps and cracks inside the vessel, and ensure that every part of the system contain electrical insulation, as well as a cooling agent. The liquid inside the vessels is pressure compensated to match the external seawater pressure. This design inherently reduce the wall thickness of the vessel, down to e.g. ≈ 10 mm [3], and reduce the cost of the component considerably. In addition, the reduction in steel material may significantly lower the weight of the component, easing its transportation and installation. Reduced wall thickness further increase the heat convection between the vessel and the external environment, simplifying the cooling system of the component. Finally, dielectric liquid is by its very nature a well-suited cooling agent, ensuring a safe operating environment for the electronic components. This technology is termed *Pressure Tolerated Power Electronics (PTPE)*.

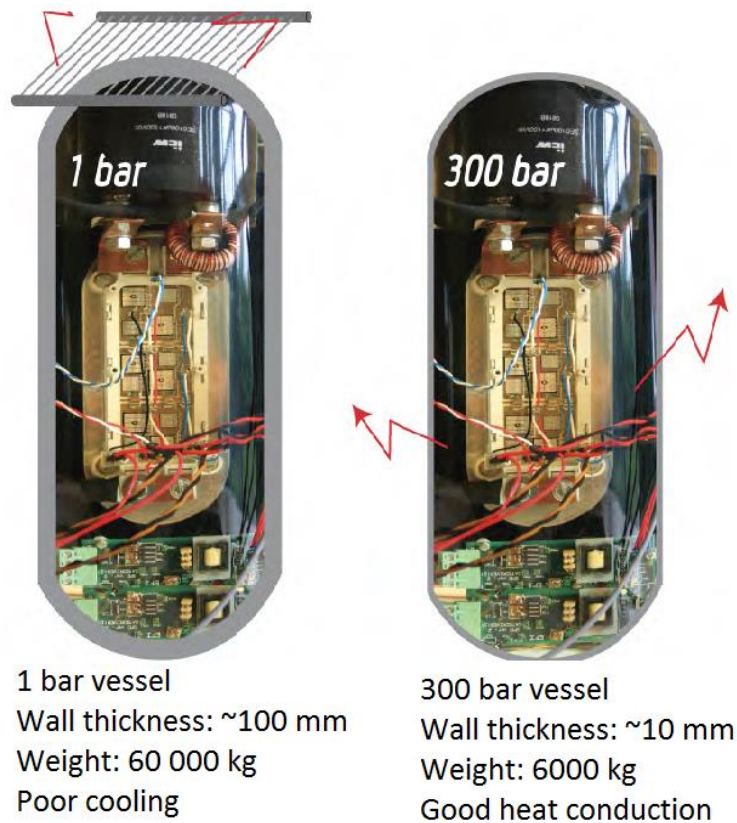


Figure 1.1, Subsea power electronic vessels [3]

PTPE is however, an immature technology branch, and several tests must be conducted before the systems can be made commercially available. Material and components inside the vessel must be able to withstand an environmental pressure up to 500 bars. In addition, the components must not react with the dielectric liquid in such a way that the material is deteriorated and damaged. Previous tests [1] have studied the effect of pressure on several different electrical components. They have observed that the mechanical stress applied by the pressure when, exceeding 300 bars, can damage some capacitors, IGBTs and optical fibres. However, the electrical properties of the components, such as permittivity and conductivity, are not alternated significantly. In this regard, components may need to be custom designed, in order to tackle the high pressure.

Many of the components in the subsea plant has a large energy rating, hence the voltage applied to the converters has a high rating as well. In this regard, some parts of the PTPE will and may experience high electrical field stress. If the electrical field reaches a certain threshold partial discharges (PD), or worst-case, breakdown may occur in some parts of the system. Such phenomenon may permanently damage parts of system, leaving the component unfit for its tasks. Areas with sharp edges, small bumps and narrow points may develop a strong electrical field, $E > 10^6$, even if the applied voltage is considerably lower. More specifically, it has been reported that parts of IGBTs experience high field stress due to complex geometry. Due to the confined space inside the vessel, it is crucial that the components are thoroughly electrically insulated.

As mentioned, it is favourable that each segment of the subsea equipment is self-monitoring. Routine test should be able to reveal if and where PD occurs in its system, in order to indicate if the system is driven to hard or if there is an immediate risk of electrical breakdown. Electrical measurement of PD is a well-established method. PD signals are registered as relative small current pulses carrying a fixed amount of charges, usually in the range 1 pC – 5 nC. Several specialised devices has been manufactured to register and measure fast transient PD signals, such as *Omicron* and *Power Diagnostix ICM System*. However, determining the source of electrical PD signals may be difficult in complex circuits. PD can be initiated several places simultaneously, as well as current signals from stray capacitance, fast switching and other noise sources is sometimes difficult to separate from PD when only studying the electrical signal. Is there an alternative way to register the initiation point, frequency and magnitude of PD activity in PTPE?

1.2 Problem Description

It is observed that PD in dielectric liquids develop into streamers, which emit light [4]. This thesis studies the relationship between emitted light and PD magnitude for several different candidate liquids. If there seems to be a correlation between photon activity and PD, this information may be utilized in a system to identify/monitor PD activity in otherwise complex circuits.

Most of the work is experimental, and consist of constructing a noise free test-circuit, with the ability to force initiate and measure PD-activity. PD signals are measured electrically using the *Power Diagnostix ICM System* in combination with an oscilloscope, while photon activity (light) is registered by a *Hamamatsu Photo Multiplier Tube (PMT)*. A point-plane electrode configuration inside an oil-filled test-cell is used to set up a highly divergent electrical field in the dielectric liquid.

1.3 Limitations

This thesis focuses on studying the connection between light emission from PD and PD charge magnitude. The major crucial parameters are electrical field strength, dielectric capabilities and molecular structure, given by the dielectric liquid. Only two groups of PD signals/streamers are studied: small negative PDs in negative half period of the AC signal, and large positive PDs in positive half period. The experiments does not consider the effect of pressure on PD behaviour. Hence, all test are conducted under atmospheric pressure conditions, 1 atm. Further, all test are performed with applied 50Hz controllable HVAC. Omitting the effect of rise time and DC-conditions on the development of PDs.

2. Theory

Partial discharge development is related to the electrical field. PDs increase in development rate and strength as the field increase above a threshold. Under sufficient AC conditions, PDs are initiated with both positive and negative polarity. The governing mechanisms for the development of PDs depend on geometrical layout, dielectric properties in the insulating medium and applied voltage.

As PDs occur in insulation, energy is released. Some of this energy is freed in the form of light. The amount of photons released depends on the strength of the partial discharge and in what material the PD occurs.

This chapter is meant to explain the physics behind development of PDs in liquid insulation across a point-plane gap, and mechanisms governing for emission of light from the mentioned insulation.

2.1 Partial Discharge

As defined by IEC 60270, a partial discharge (PD) is a localized dielectric breakdown of a portion of a solid, liquid or gaseous electrical insulation system under high voltage (HV) stress, which may or may not occur adjacent to a conductor.

In general, PD is an unwanted effect in electrical systems due to its capacity to deteriorate and damage electrical components and dielectric insulation. However, liquid dielectrics is considered self-healing. After a PD appear in the liquid, it will return to its original state. Nevertheless, some of the dielectric may have become contaminated. If several PD's occur over a longer period, the liquid dielectric may lose its dielectric capabilities, thereby risk complete breakdown and malfunction. PD also represent power loss in the system, which leads to economic losses for the operator of the given component.

The difficult nature of studying liquid insulation, compared to gas, manifests itself by the formation of gaseous bubbles inside the dielectric, ionization of molecules as well as the viscosity of the fluid.

All PDs studied in this thesis are self-quenching. This effect is due to the geometrical point-plane electrode layout chosen for the experimental work, in combination with the AC voltage levels utilized. By studying only self-quenching PDs, the PD signals are seen only as current pulses in the measuring circuit.

2.1.1 PD Development in Liquids

Development of PDs in liquid dielectrics is a complex phenomenon, which is not yet fully agreed upon in literature. However, it is widely regarded that electrons are the main driving charge carrier in all PDs. If free electrons in the bulk is exposed to a sufficiently strong electrical field, an electron avalanche may be initiated. In order for this to occur free electrons has to

be released into the bulk of the liquid by some sort physical mechanism. Five mechanisms for electron injection is mentioned here.

Field emission in liquids is a form of electron injection at the cathode, and is considered one the main mechanisms for charge injection into liquids. If the electrical field is sufficiently strong, electrons may be freed from the lattice at the electrode, and pushed into the bulk. The field strength required is dependent on the material of the electrode, but is often in order of 10^7 - 10^8 V/cm [5]. Such field strength may occur near small bumps, points and other irregularities at the electrode, and create a highly divergent electrical field, even at relative low applied voltage levels (2-5 kV). The energy required to remove an electron from the metal lattice is known as the Fermi level, given by the work function (W_a). The freeing of these electrons are also known as “tunnel effect” and is explained by Fowler-Nordheim [5]:

$$j = CE^2 \exp\left[-\frac{D}{E}\right] \quad \text{Eq. 1}$$

Where j is the current obtained by field emission and E is the electrical. C and D are constants given by the atoms. As seen by Eq. 1 the field emission is independent of temperature, however, this is not valid for high temperatures. As temperatures exceed (1500-2000 K) the current created at the cathode is governed by thermionic emission as well as field emission. This combined electron injection is given by the Schottky equation [5], but will not be discussed further here.

Suspended Solid Particles may be present in the liquid, such as fibres from paper insulation or loose pieces of other solid dielectrics. Such particles can become polarized due to the electrical field, and thereby experience an applied force. If ϵ and r is the particles permittivity and radius respectively and ϵ_{liq} the permittivity of the liquid, then the applied force to the particle will be: [5]

$$F_e = \epsilon_{liq} r^3 \frac{\epsilon - \epsilon_{liq}}{\epsilon + 2\epsilon_{liq}} E \nabla E \quad \text{Eq. 2}$$

These particles will move towards the area where the electrical field is strongest, as long as $\epsilon > \epsilon_{liq}$. If the field is uniform, the particles may align and cause breakdown due to the particles essentially acting as a conductor. If the field is non-uniform the particles may align in the area with the strongest field, and thereby initiate PD due to extreme field stress. This electron injection is conducted by field emission; basically, the same phenomenon as discussed above, but the suspended particles in the bulk amplifies the field strength. It should be noted that the movement of particles in the electrical liquid field is also dependent on the viscous drag, given by Stokes relation (which will not be given here).

Cavity Breakdown in liquids shares a similarity to void breakdown in solids. Bubbles are filled with gas that generally have lower permittivity then the liquid in which it is submerged. The bubbles are formed by:

- Gas pockets on the electrode surface
- Changes in temperature and pressure
- Electron collision causing gaseous products
- Liquid vaporization by corona-type effects

As the electric field is applied across the cavity, electric breakdown may occur due to high field stress inside the bubble. The electric field inside a spherical bubble is given by K.C Kao [5] as:

$$E_b = \frac{3 E_0}{\epsilon_{liq} + 2} \quad \text{Eq. 3}$$

Where E_b is the field inside the cavity, E_0 is the applied field in the liquid and ϵ_{liq} is the permittivity of the liquid.

As for solid dielectric erosion breakdown, the small bubbles can be modelled as series capacitances inside a healthy dielectric medium. Using the A-B-C model for PD in solids [6] the size of the electrical discharge may be calculated inside the bubble.

Photoionization

Electrons may be released into the bulk by ionization of the molecules in liquid. Some photons can acquire enough energy in order to create a cation when colliding with some molecules. As a cation is created, an electron is freed from the molecule. Such high-energy photons can be found from relaxation of other excited molecules as well as from inserted photons into the liquid by cosmic radiation or other instalments.

Field ionization at anode is another form of ionization in the bulk, freeing electrodes. If the electrical field is strong enough, the molecules in the bulk may experience an applied force sufficiently large to release electrons from the molecules. This phenomenon is described by Poole-Frenkel [7].

2.2.2 PD Propagation and Streamer Phenomenon

As the initiation process of PD has occurred in the liquid, a local electronic avalanche is produced. Whether the initiation is achieved by field emission at cathode, photoionization, cavity breakdown or field ionization at anode, previous studies [8] [9] have experienced that these initiation impulses occur very rapidly (\approx ns). This rapid initial electron avalanche creates a shockwave inside the liquid, which forms a micro cavity channel of vaporized dielectric medium. The channel, also known as a *streamer*, propagate through the liquid along the electrical field, containing a conductive ionized plasma.

The streamer will propagate into the liquid for as long as the electrical field is strong enough to energize the leading electrons in head of the stream, supplying enough energy to keep

ionizing new molecules. The streamer may also be conducted by photoionization. The energy needed ionize a molecule is given by [5]:

$$eE\lambda = ch * v \quad \text{Eq. 4}$$

Where e is electron charge, E is the applied electric field, λ is the electron mean free path in the dielectric medium, $h\nu$ the amount of energy lost in ionizing a molecule and c an arbitrary unit.

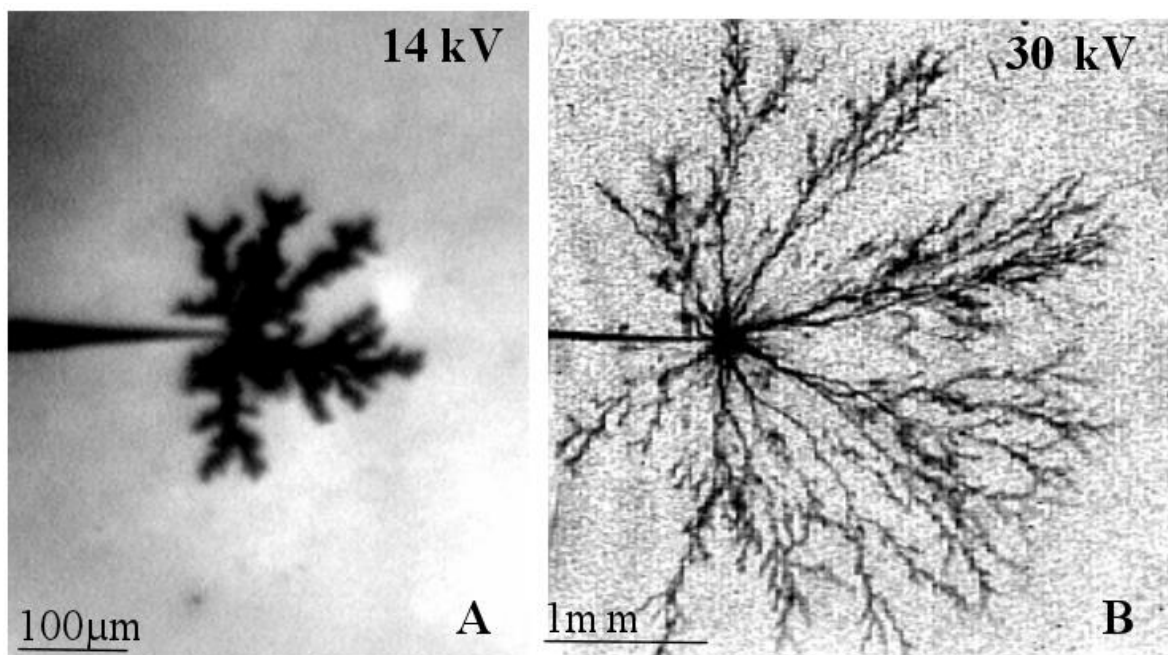


Figure 2.1. A: Small negative streamer (bush). B: Large positive streamer (filament).

A “tree” formation is seen as the streamer propagate itself into the liquid. In a highly divergent field, the streamer will quench before bridging the two electrodes. The streamer is termed either as positive or negative, depending on the polarity of the applied voltage of the source electrode.

Negative streamers has in general a lower inception voltage then the positive streamers. The most common negative streamer is observed as a small PD, piercing not too far into the liquid. Typical charge magnitude for such streamers are 0.5-70pC. The physical periphery of these streamers are seen as numerous close conductive channels, often referred to as a “bush”.

Positive streamers normally carry a larger amount of electrical charges than the negative ones, containing more energy and propagate further into the dielectric liquid. The positive streamer are observed as filamentary with rather few conducting channels, but which in turn is more luminous then the negative ones. The streamers are further categorized by the velocity of their propagation.

2.2.3 Light Emission from PD Streamers

During partial discharges, energy is released inside the electron avalanches. The energy can be freed as either heat, sound or light. Heat release during PD has been proven by Lesaint et al. [9] as the liquid is vaporized into the plasma channel of the streamer. Previous work has observed that the streamers emit flashes of light [4]. It is been registered that the large positive filamentary streamers emit more light than the weaker negative “bush” streamers. Further, it is stated that light emitting from streamer can be divided into two separable incidents [10]:

- Light emitted from the tip/front of streamer.
- Light emitted from the re-illumination of the streamer channel.

In the front of streamer, heavy ionization is occurring as the front is propagating into the liquid. As mentioned earlier this creates a conducting plasma filled cavity channel. During the ionisation-processes electrons are released, as well as some energy in the form of photons. The radiation, intensity and amount of photons released at the tip of the streamer are governed by the molecules of the liquid in which the streamer occur, and the electrical field. More about this in section 2.5.

After a brief time lag, the streamer channel is observed to flash up. Much like observed in the stepped leader in a gas discharge (lightning). The exact reason for this behaviour inside the streamer is not precisely determined. However, it is believed that this phenomenon appears due to a breakdown of the streamer channel. The channel is filled with a conductive ionised plasma with a high density. The channels cross section expands, reducing the ratio between the density and field stress, increasing the conductivity. This allows for arcing inside the channel, and the inrush of a strong illuminating current.

2.2.4 Additives effect on PD

The addition of chemical additives in the dielectric liquids may alternate its dielectric properties. Such alternations can affect the behaviour of the streamers observed in the liquid. As discussed in [11], electron-scavenging additives will generally increase the propagation speed of negative streamers. Additives with low ionization potential (IP) has been observed to increase the speed and branching of positive streamers. N,N-dimethylaniline is an example of low IP additive.

Water content in the dielectric is another form of additive that is commonly found in many dielectrics. Moisture is absorbed into the liquid from the surroundings if the liquid container is not properly sealed off. Water has generally lower permeability and breakdown strength than dielectric liquids. Hence, considerable concentration of water will decrease the insulating capability of dielectric. However, some dielectrics are less sensitive to high water concentration, and are capable of absorbing relative large amounts of moisture without reducing its breakdown strength significantly. MIDEL 7131 is one such dielectric.

2.2.5 PD as Stochastic Phenomenon

The occurrence of partial discharges is given by several stochastic factors. As described by R. J. Van Brunt [12] the initiation process for PD are dependent on: probability of initiatory electron-injection given by field strength and geometry; dynamics of dielectric surface charging; growth rate of cavities and bubbles created by discharge activity in dielectric liquids; rate of space charges created due to field emission and ionization and memory propagation from previous PD activity. All these factors are stochastic by nature and non-independent. Leaving PD development as a stochastic phenomenon as well as having non-Marcovian behaviour.

Laue [13] found for PD in gases a connection between electron injection, electron collision and PD development. He found that the PD development time lag follow a Poisson distribution, given as:

$$\frac{n(t)}{n(\infty)} = \exp(-R_e(\Delta V)P(\Delta V)t) \quad \text{Eq. 5}$$

Here $\frac{n(t)}{n(\infty)}$ is the fraction of the discharge events that have delay times greater than t , $R_e(\Delta V)$ is the rate of electron injection into the field region and $P(\Delta V)$ is the probability that an electron initiate a PD or breakdown. Both P and R_e can be expected to increase with increasing ΔV . ΔV is given as the voltage level difference above onset voltage V_s .

$$\Delta V = V - V_s \quad \text{Eq. 6}$$

These formulas are given for PD phenomenon in gases, while for liquids the field is less explored. However, the formation of PD in liquids is also experienced as stochastic, though more complex than for gas. Considering the stochastic nature of PD development, it is difficult to predict the exact result of experimental work in this field. Variance will occur during tests, even though utilizing the exact same setup and preconditions. Some preconditions is also more or less non-controllable, such as the amount of space charges and micro particles in the liquids.

2.2 Point-Plane Geometry

The point-plane geometry is an ideal geometric design when wanting to create highly divergent electric fields. By applying high voltage to the electrodes, extreme field stress will develop approximately to the point-electrode. Meanwhile the plane-electrode experience a low electrical field compared to the point. Ensuring an appropriate gap length between the electrodes, partial discharges may be provoked near the point electrode, while avoiding complete electrical breakdown of the gap.

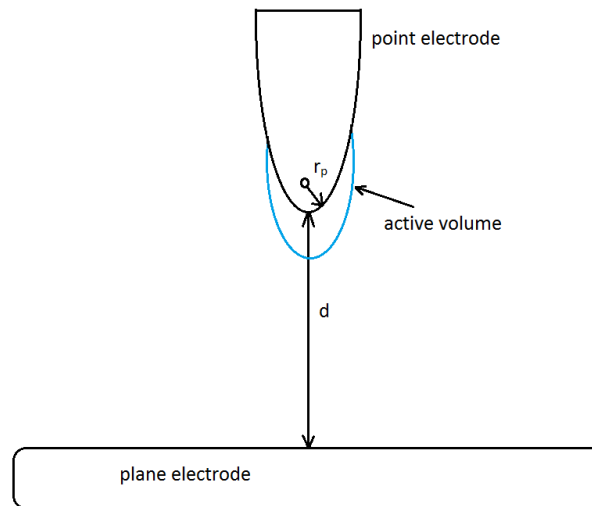


Figure 2.2, Point-plane geometry

Figure 2.2 illustrate the point-plane geometry. r_p is seen in as the radius of curvature of the tip of the point electrode. The active volume, as indicated by the blue line, is the section of the point electrode contributing significantly to the field stress near the tip.

Calculating the electrical field between the electrodes in the point-plane geometry is difficult using Cartesian coordinates. By utilizing a thin wire as the point-electrode, the electric field near the point can be modelled as a hyperboloid, as mentioned by Lundgaard et al. [4] [14]. Doing so, several symmetries occur encircling the point electrode. Leaving the most interesting section to be the area where the electrical field stress is strongest. This are is located precisely near the tip of the point electrode, and along the Cartesian z-axis towards the plane electrode. The electrical field at the tip of the point electrode is then given as [14]:

$$E_{tip} = \frac{2V}{r_p \ln\left(\frac{4d}{r_p}\right)} \quad \text{Eq. 7}$$

Where $V [V]$ the applied voltage at the electrode, $r_p [m]$ is radius of curvature at wire tip and $d [m]$ is distance between the two electrodes, same as depicted in Figure 2.2. The field strength near the tip is much more sensitive to changes in the tip-radii (r_p), then to electrode distance (d). Increasing the tip radii from 5 to 6 μm results in a filed reduction of 15%, while increasing the distance from 20 to 21 mm change E_{tip} by 0.45%. The tip of the point electrode may experience changes during tests. Etching at the tip may occur during high field stress and ionization processes. The tip can also be altered by potential breakdowns, damaging and dulling the tip.

Figure 2.3 displays the general behaviour of the electrical field across a point plane gap. The blue line (intersection-points highlighted) illustrates that the electrical field is nearly unaltered by the reduced gap distance.

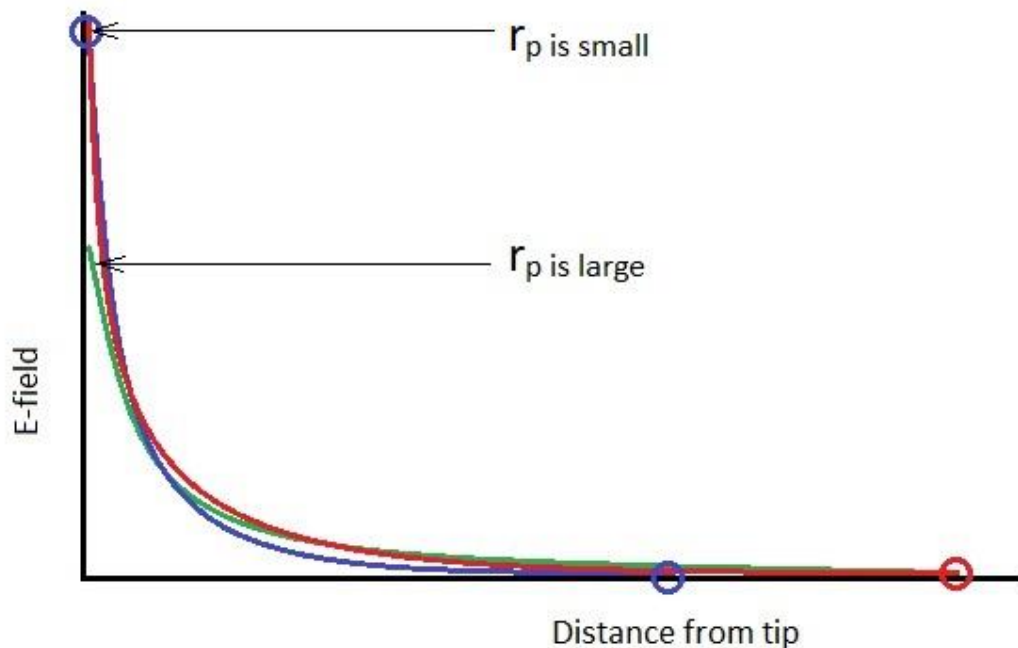


Figure 2.3, General electrical field strength compared to tip radius and electrode distance.

2.3 Space Charges in the Liquid Dielectrics

As AC voltage is applied to the electrodes of a point-plane gap, build-up of space charges will appear in the bulk of the dielectric liquid. Space charges are either free charges or polarised molecules/particles in the bulk. Four governing mechanisms polarise dielectric mediums [6]:

- *Electronic polarisation.* Applied electrical field distorts the electrons in the dielectric atoms. Effectively creating a temporary dipole, proportional to the applied field.
- *Ionic polarisation.* Ionic bonded material aligns to the applied electrical field, pulling the positive ions in one direction and the negative ions in the opposite.
- *Orientation polarisation.* Some molecules are permanent dipoles. These molecules align to the applied field.
- *Interfacial polarisation.* Cavities and impurities can acquire free electrons in the dielectric, due to the applied field. Gathering of such charges creates a surplus of either polarity on the interface.

The electronic and ionic mechanisms are considered instantaneous while the orientation and interfacial polarisation need time to develop. Viscosity in liquids makes the movement of space charges slower than in gases. [4] Assuming an ion mobility $\mu=10^{-9}[\text{m}^2/\text{Vs}]$ and a field $E=6 \cdot 10^8 [\text{V/m}]$ the ionic movement speed is $v=0.6 [\text{m/s}]$. As AC voltage is applied, the space charges

will not have time remove itself from the vicinity near the tip. Causing a congestion of space charges near the tip.

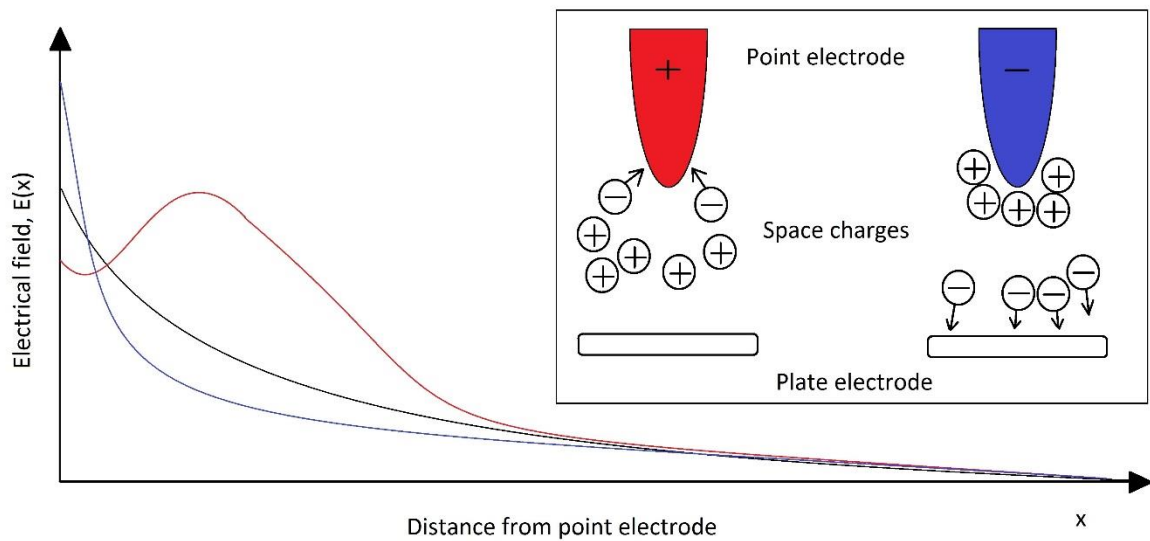


Figure 2.4, Electrical field alternated by space charges

Figure 2.4 illustrates the effect of space charges near the tip of the point electrode. The black line is the expected electrical field spread into the dielectric liquid, ignoring space charges. The red and blue lines correlate with the red and blue electrodes respectively. At the positive (red) electrode, the negative, and fast moving, charges will be dragged towards the anode, leaving the positive charges behind. As displayed in Figure 2.4, the electrical field near the tip is weakened by this effect, compared to the normal field (black line). In the area near the positive space charges, the field is increased. When negative voltage is applied to point electrode (blue) the negative charges are propelled by field into the liquid. Leaving only the slower positive charges, which are also dragged towards the cathode. The resultant electrical field is here increased near the electrode tip, but drops faster with increased distance, compared to the expected normal (black) curve.

The effect of space charges in the dielectric is important to understand when studying PD in liquids. The charges can alternate the electrical field to such an extent that PD or even breakdown may occur at lower/higher voltage level than anticipated. Lundgaard and Kyrkjeeide [4] postulated a hypothesis that the occurrence of several small negative PDs, left a surplus of negative space charges in the bulk. These space charges alternated the field to such an extent that the electrical field may reach levels for large positive PDs.

2.4 Oil Light Emission

If a molecule is supplied with external energy, some physical phenomenon may take place. One of which is excitation of electrons in the molecule. Without going into too much depth, this revolves around electrons in some of the atoms in the molecule being “kicked” up to higher energy level. The electron may jump up to an electron shell of higher order, before

falling back to its original state, relaxation. The amount of energy needed to excite a specific electron to a given state is fixed for each molecule. However, one molecule may have several different excited states. This is due to different electrons being excited, and the possibility for the same electron to reach different electron shells/energy states. During the relaxation process, the excess energy from higher electron shell is released from the molecule, mainly in the form of light. The wavelength from the emitted light due to relaxation is unique for each energy state of the specific electron.

If the amount of supplied energy to the molecule is sufficient, the electron in the molecule is not excited but permanently released from the structure. Creating an ionized molecule/cation. As streamers propagate into the bulk of the dielectric liquid, heavy ionization occurs at the tip of the streamer. The ionization potential (IP) for a molecule is termed as the amount of energy needed to ionize a molecule, releasing electrons from its structure and create a cation. Ionization can occur in the form of electron collision, known as impact ionization. Photoionization occurs when photons with sufficient energy is absorbed into the molecule, ionizing it. The IP of a molecule A is given as [7] [15]:

$$IP = U_{A^{+}+e} - U_A \quad \text{Eq. 8}$$

Where $U_{A^{+}+e}$ it the interaction energy between an electron and the molecular cation (A^+) in an electric field at the dissociation barrier. Dissociation barrier meaning the energy level at which the electron parts way from the rest of the molecule. U_A is the energy of molecule A in the electrical field. Previous work [7] have acquired a more practical form of Eq. 8, given as:

$$IP = IP_0 - 2 \sqrt{\frac{E}{\epsilon_r}} \quad \text{Eq. 9}$$

Here IP_0 is the IP at zero applied field, E is the electrical field and ϵ_r is the relative permittivity of the material. As seen from Eq. 8 and Eq. 9 the IP is reduced as the electrical field increase.

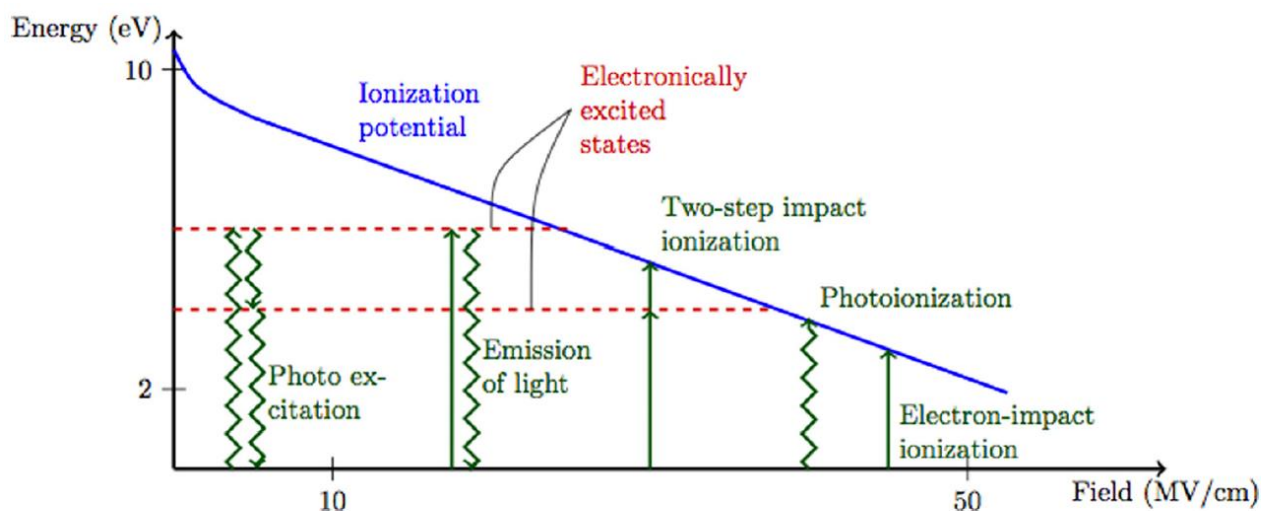


Figure 2.5, IP level versus electrical field [7]

Figure 2.5 illustrates the IP level, blue line, as a function of the applied electrical field to an arbitrary molecule. The green straight lines display different ionization processes, however, all forms for ionization may appear at any given field strength. The given placement of the green straight lines are arbitrary, and serves to give a clear presentation. The green wavy lines are representations of light. The scales on the axis are arbitrary.

As indicated Figure 2.5, several levels of excitation may be present in a single molecule. As the electrical field increase the levels demanding the highest excitation energy disappears, due to the lowering of the IP level. For some molecules, one will eventually end up with only a two state molecule. The two state molecule is in either the ground level state or the ionized level state. All other excitation levels have then been suppressed by the IP. If the time between excitation and relaxation is long compared to the frequency of electron impact or photon absorption, the molecule can experience a two-step ionization.

3. Method and Experimental Work

The experimental work done in this thesis has the overall motivation to get a better understanding of PD in dielectrical liquids. Therefore, a test setup is built to easily provoke PDs activity at a fixed point, while allowing for easy and precise measurement.

High voltage AC, 15-29 kV,rms, is applied to a point-plane electrode configuration. The high voltage part of the system is built inside a Faraday cage. Hence, ensuring safety for the operator, reduce electrical interference from the surroundings as well as darkening the environment around the electrode gap. PD signals are measured electrically using the *Power Diagnostix ICM System* and a *Tektronix DPO5104 Oscilloscope*. Light emission from PD are registered by a *Hamamatsu R1635 PMT* in combination with the same oscilloscope.

Supply voltage is given great emphasis on it being noise free, possible to alternate frequency and voltage level. Hence, the circuit is designed to operate under resonant conditions, isolated from the power grid. A model, built in *MATLAB SIMULINK Sim Power Systems*, is used to help get a clear understanding of the behaviour of the test setup, and to indicate the power rating needed for some components.

3.1 Laboratory Setup

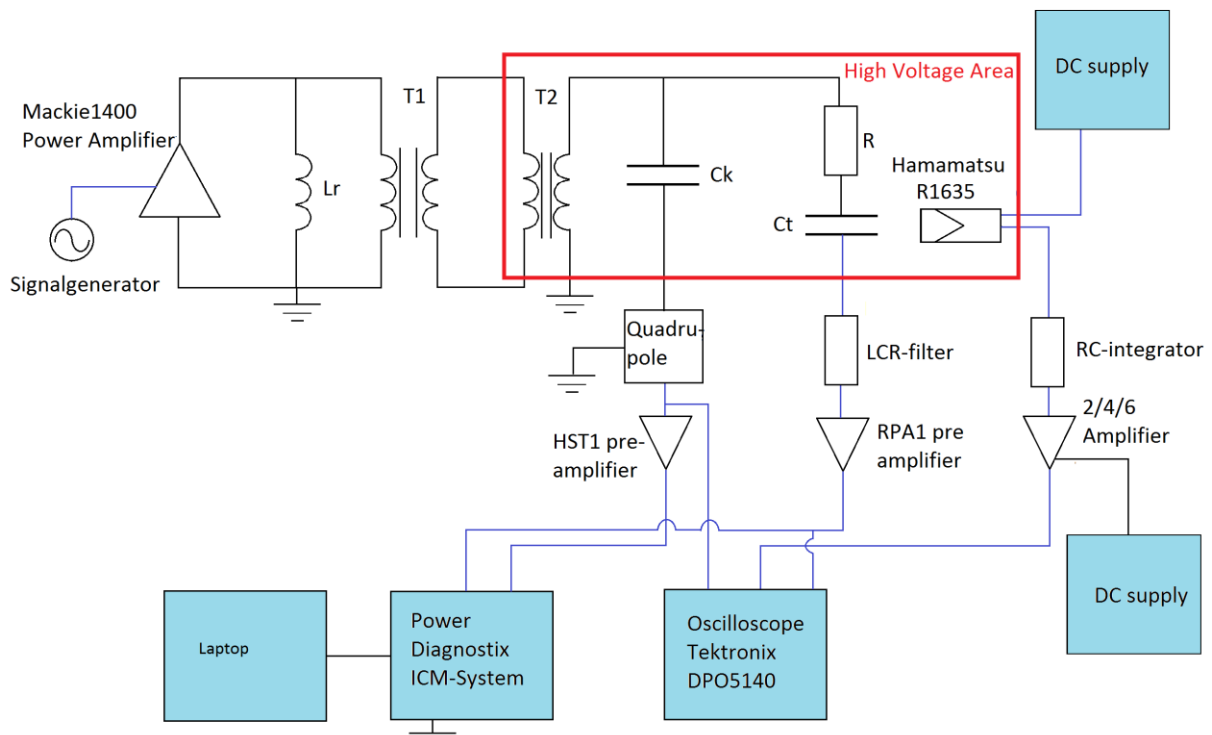


Figure 3.1, Complete test circuit

Figure 3.1 illustrate the complete test circuit used during the experimental work. Blue lines indicate coaxial BNC cables, while black lines are one directional connections. The red rectangle illustrate the Faraday cage where the high voltage operates. The other elements in Figure 3.1 are:

- L_r : 3.52 mH, balancing inductance
- T_1 : 20/40/60:220 isolation transformer
- T_2 : 220:50 000 high voltage transformer
- C_k : 1023 pF, PD free coupling capacitance
- C_t : Test cell with point-plane electrodes. Measured capacitance 0.1 pC
- R : 35,15 k Ω , current reducing resistance

The general behaviour of the test circuit, displayed in Figure 3.1, is given here. Note, crucial components and concepts are more thoroughly described in the following sections.

A *Wavetek* signal generator creates a sinusoidal AC signal, with controllable frequency and amplitude. The signal is fed into the *Mackie1400 High Current Amplifier*, which amplifies the signal. Balancing inductance L_r has the function to compensate for the capacitive impedance seen by the Thevenin equivalent in the circuit. Further, the signal is transformed up to a higher voltage level, first by T_1 then by T_2 . The total voltage transformation done by T_1 and T_2 is:

$$n = \frac{220}{40} * \frac{50000}{220} \quad \text{Eq. 10}$$

$$n = 1250 \quad \text{Eq. 11}$$

The high voltage signal is divided between the coupling capacitor, C_k , and the test cell, C_t . A *Power Diagnostix Quadrupole* is connected in series with C_k . The quadrupole earth the HV and supply a scaled down version of the HVAC signal (1/1000) into the oscilloscope and the *ICM System*. The ICM signal passes through a *Power Diagnostix HST1 pre-amplifier*. The test cell stray capacitance is previously measured to be ≈ 0.1 pF. During normal testing conditions, approximately zero current would cross the electrode gap. However, a resistance, R , is connected in series to reduce current in the case of breakdown and arcing. A LCR-filter in series with the test functions as a band-pass filter for PD signals into the ICM system.

The *ICM System* register PD pulses and HVAC. PDs are displayed in a phase-amplitude plot. The PD signal into the ICM is also fed into the oscilloscope, which display the PD as voltage pulses. The PMT is driven with a controllable DC source. The PMT output current pulses created by photon activity. PMT singles are integrated by a custom RC-integrator to portray several fast transient light pulses as one signal. The PMT signal is displayed on the oscilloscope.

3.1.1 Test Cell

The 1.6 L test cell, seen in Figure 3.2, is used during the experimental work. The same/similar test cell configuration is previously utilized by Lundgaard, Ingebrigtsen et al. [16] [14] [4]. The

cell contain a point-plane electrode configuration used to create a highly divergent field. The 90mm diameter plane electrode is connected to a micrometre screw. The gap distance between the point and the plane can be adjusted by operating this screw. Two symmetrically aligned, 131mm diameter, borosilicate windows form the two flat surfaces of a cylinder. A grounded metal shield is placed around the walls of the cell, in order to achieve a more uniform and defined stray capacitance.

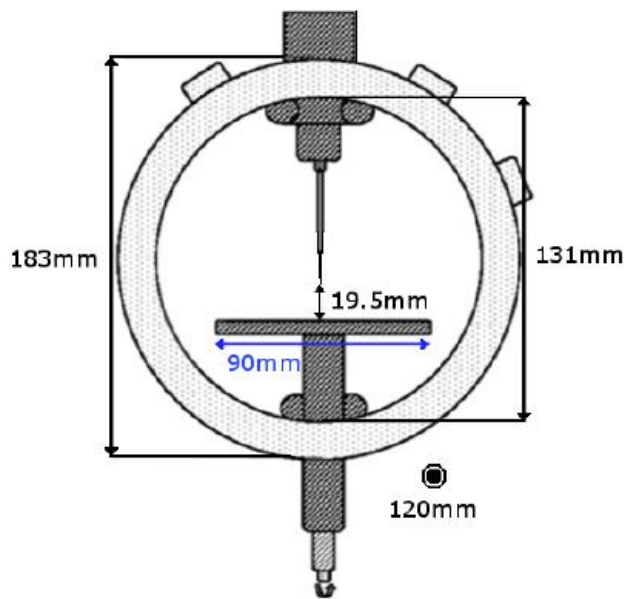


Figure 3.2, Test cell configuration [16]

The point electrode is illustrated in Figure 3.3 [14]. (1) Huber Suhner 11 SMB-50-2-41/111 NE, (2) threaded steel tube, (3) insulating plastic tube, (4) chromatograph needle, (5) 100 μ m diameter tungsten wire. The tip of the wire is electrochemically etched down to a small radius of curvature, r_p , at the tip.

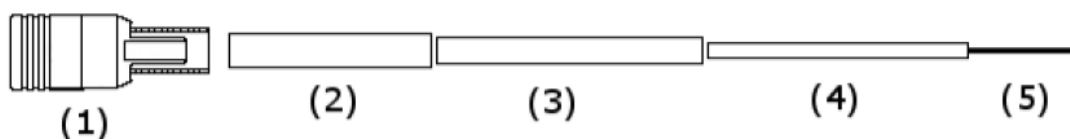


Figure 3.3, Needle configuration [14]

3.1.2 Signal Generator and Power Amplifier

A 4 MHz Model187 Wavetek pulse/function generator is used to create a pure sinusoidal voltage signal. The generator can deliver 20V peak-peak, and vary its frequency between 0-4MHz. The signal generator is capable of delivering several different types of voltage signal, including sinusoidal, square and triangular, with and without a DC offset. However in this thesis only sinusoidal were utilized.

A Mackie M1400 FR Series power amplifier is used to amplify the generated sinusoidal signal. A custom XLR-banana cable is constructed to transfer the signal from the BNC output of the signal generator into the XLR input connection of the amplifier. The amplifier is capable of delivering up to 1400 W and has several different amplification/gain settings [17]. Max gain for the amplifier is however 30dB, effectively multiplying the signal by:

$$30[dB] = 20 \log(x) \quad \text{Eq. 12}$$

$$x = 31.62 \quad \text{Eq. 13}$$

All though originally designed to operate as a professional loudspeaker amplifier, with the ability to cut off high-level transient signals, the output signal is of very high quality. A 2Ω load should be connected to the output of amplifier when operated in MONO mode. This, to avoid potential short circuit, large currents and overheating of the amplifier. Further, the amplifier operates as a smart device with its own internal cooling and warning system [17].

3.1.3 Power Diagnostix ICM System

The *Power Diagnostix ICM System* is a specialised automatic partial discharge detector. The apparatus is very flexible, and can be utilized in several different settings. Its sensitivity is <1pC, if tuned correctly to measuring circuit. The input connections contain signal amplifiers, which can be modified to fit the signal strength studied. Most of the hardware uses BNC-connections to transfer signals. In addition to internal amplifiers, external preamplifiers and quadrupoles are connected near the test object, hence achieving highly sensitive measurements. A wide array of different preamplifiers and quadrupoles are available, with different specifications regarding the studied circuit. In the setup used in this thesis a RPA1 preamplifier is used, with a signal gain of 0/20/40dB and a bandwidth of 40-800 kHz.

The device is operated by an externally connected laptop, running the *Power Diagnostix* custom software programme *SysMux*. All internal settings of the device is controlled by the software, as well as operation of the external preamplifiers gain settings. All gathered data is collected and displayed in the software interface. PD signals may be displayed in several different ways. However, in this thesis the measurements are given as n-θ-q plots. n is the number of discharges, θ [rad/deg] is phase placement and q is the size [pC/nC], see [18] for mote information.

3.1.4 Photo Multiplier Tube

A R1635 Hamamatsu PMT is used to register light emission, i.e. photon activity inside the dielectric liquid. The R1635 PMT is illustrated in Figure 3.4. A negative polarity DC voltage is applied to the photocathode, *K*. As photons collide with the photocathode, electrons are released into the tube. The released photoelectrons are accelerated into the first of a series of dynodes, *DY1-DY8*. The dynodes has incremental increasing positive voltage regarding the cathode. As the electrons collide with the first dynode, *DY1*, more electrons are released and accelerated towards the second dynode. This process is repeated for all dynodes before reaching the anode, *P*, causing a cascade effect, amplifying the current out of the PMT. Due to instability at the photocathode, a certain amount of electrons may and will be released into the tube without the presence of photon activity. The current developed without light is known as *dark current*. Dark current is a purely stochastic phenomenon, and depends on the applied voltage, material of photocathode and ambient temperature. When using a PMT it is important to understand and acknowledge the effect of dark current, and be critical to whether the measured output signal is a real light measurement or not.

The R1635 is an 8-dynode stage PMT, with an amplification rating seen in Figure 3.5. The tube used here is slightly modified, where the window material in front the photocathode is made up of quartz instead of borosilicate glass. Thus, increasing the range of the spectral response to include a wider range of the infrared light, 180-650nm. It is a head-on PMT with a bialkali photocathode know for high sensitivity and low dark current. Max supply voltage for the tube is 1500V DC. The output signals produced at the PMT anode, *P*, are very fast, with a rise time $\approx 0.8\text{ns}$.

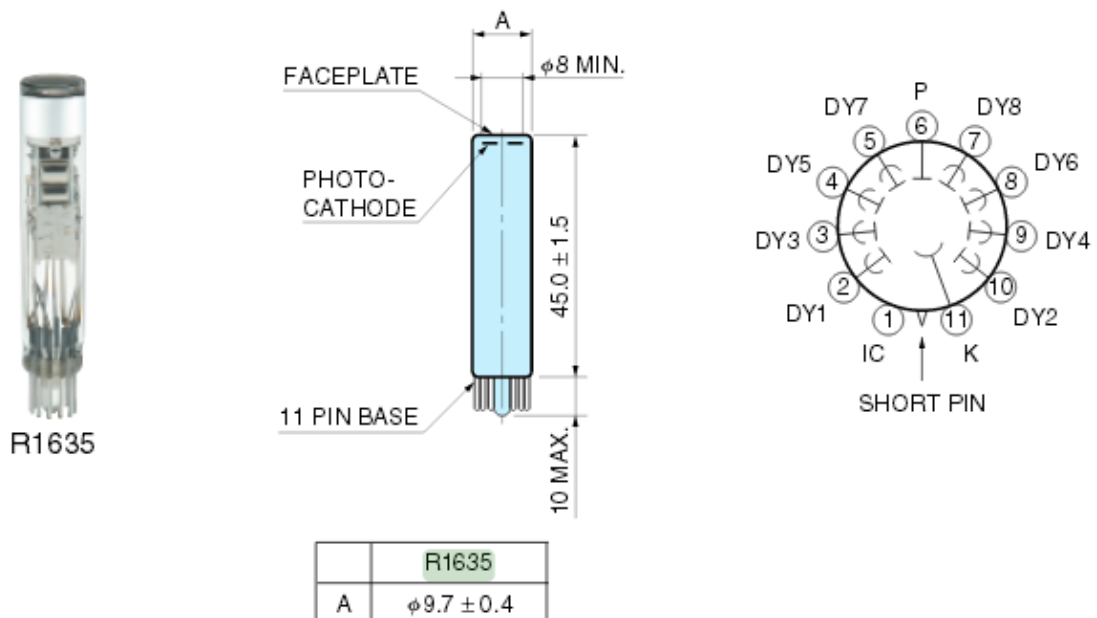


Figure 3.4, R1635 PMT

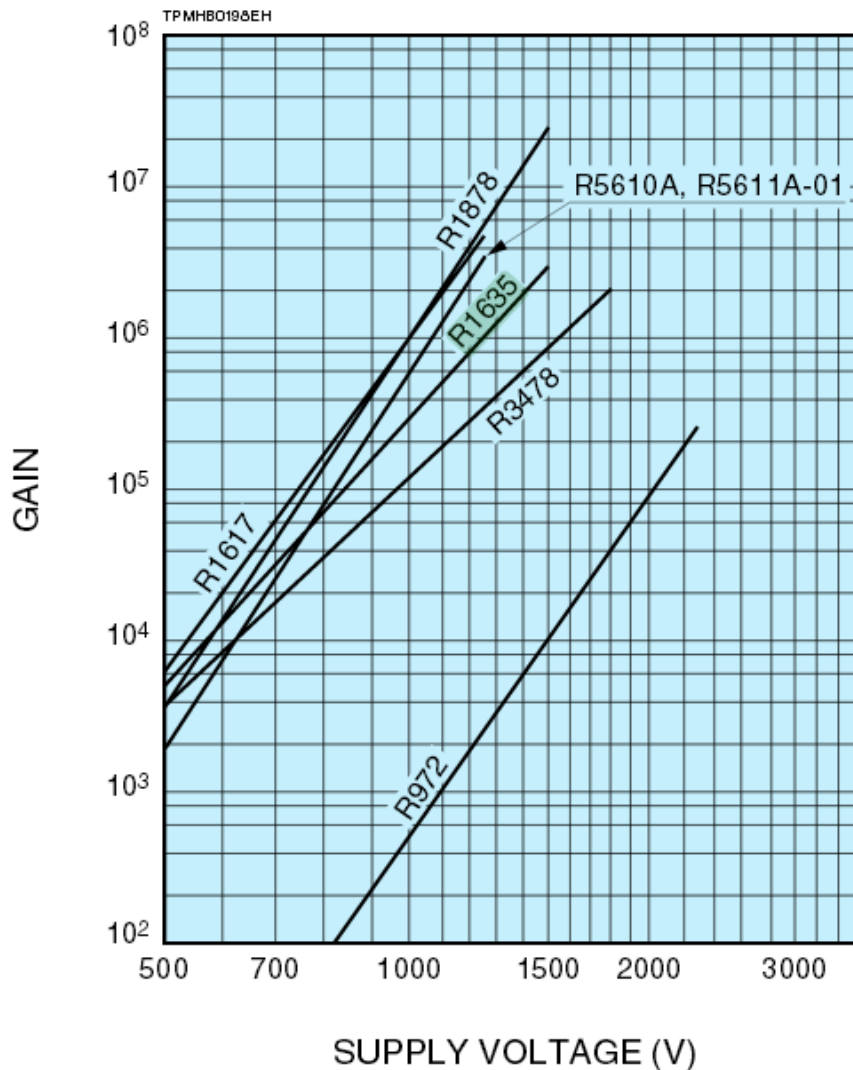


Figure 3.5, PMT Gain Characteristics [19]

3.1.5 RC-integrator and 2/4/6-preapmlifier

The output signal from the PMT is, as mentioned, very rapid. The signals are also relative small in amplitude. Electrical signals into the ICM System are less transient, rise time $>1\mu\text{s}$, and of greater magnitude. Hence, it is very impractical to compare signals from the ICM and PMT, when displayed on the same oscilloscope simultaneously. To compensate for these differences, a RC-integrator and a voltage amplifier is connected in series with the PMT, as depicted in Figure 3.1.

A 2/4/6 Physical Acoustics Corporation Voltage Preamplifier is used to amplify the PMT signal. The voltage gain can be adjusted to 20/40/60dB, and is easily selected by adjusting a switch. Input impedance is 10k Ω /15pF. The preamp needs a 28V DC supply in order to operate [20].

A simple custom RC-circuit is constructed. A 945pF capacitor is connected in parallel with an 11k Ω resistance. Combined with the input impedance of the preamplifier the time constant of the integrator circuit becomes:

$$\tau = RC \quad \text{Eq. 14}$$

$$\tau = 4.95\mu s \quad \text{Eq. 15}$$

This time constant fits well with rise time for the ICM system signal. However, it is important to be aware that the light signal now displayed on the oscilloscope is affected by this integration. The signal displayed on the oscilloscope is most likely a series of several light pulses in rapid succession, rather than one single pulse.

3.1.6 Oscilloscope

A *Tektronix DPO5104* 4 channel oscilloscope with sampling rate up to 10 GS/s and a bandwidth of 1GHz is used to sample all the different measuring signals simultaneously. The oscilloscope allows for advanced trigger functions, easing the process of extracting the wanted data from the experiments, [21].

3.2 Resonance Circuit

The usage of a controllable signal generator, instead of a variac introduce several advantages. The generator is isolated from the net; hence, it does not transfer net noise into the test-circuit. Further, the signal generator allows varying frequency and waveform of the signal as needed. The test-circuit built here is designed to operate at resonance, while being capable of varying the frequency. Resonance implying that at a certain frequency, the impedance “seen” into the Thevenin-equivalent from the source is purely ohmic.

$$Z_{th} = R \quad \text{Eq. 16}$$

This is a complicated design, since impedance in the circuit changes as the frequency varies. However, the benefits from achieving resonance is rather significant. Due to the impedance being purely ohmic there will be no phase shift between voltage and current. This eases some of the calculations and measurements when analysing the collected data. The pure ohmic conditions does so that no power is “wasted” as reactive power, Q. In addition, the supplied current into the test setup can be as low as possible. In the case of breakdown inside the test-cell, an arcing occur across the electrodes. The arcing will, for the brief moment it lasts behave as a conductor, which will dramatically change the impedance equivalent of the circuit. If the circuit is finely tuned the voltage supply to the arc will be cut off. Hence, extinguish the arc as soon as the AC voltage crosses zero.

In order to calculate the proper circuit elements needed to achieve resonance, a *MATLAB Simulink* model is created. *Appendix A* display the final model of the system. Short circuit and open circuit tests were performed on the two transformers T₁ and T₂, seen in Figure 3.1 and

Appendix A. The magnetization and winding impedance are calculated for the transformers, and are available in Appendix B. Several simulations and test are performed in the model, in order to predict the voltage/current behaviour. This helps determine the power rating for the components used in the test setup.

3.3 Selection of Dielectric Liquids

Four dielectric candidate liquids are tested in the experimental work.

- Nytro 10XN
- MIDEL 7131
- Galden HT200
- EXXSOL D80

They are all chosen based on their molecular structures, which are fundamentally different for each liquid. It is expected that the PD behaviour and light emission from the liquids will vary, due to their differences.

The water content are tested using the Karl Fisher measurement, performed by a 737 *Metrohm KF Coulometer*. Several 2ml samples of the liquids are tested, together with a Hydranal solution to determine the amount of moisture given as μg by the instrument. From these measurements, water content in ppm can be easily calculated. However, only two of the liquids are tested for water content, due to technical problems.

3.3.1 Nytro 10XN

Nytro 10XN is a transformer oil solution consisting of several different molecular structures. Naphthenic hydrocarbons are one of the dominating compounds in liquid. The general naphthenic formula is given as C_nH_{2n} , and appears as saturated cyclic structures. Alkane is another structure found in the oil. Alkane are linear saturated hydrocarbons, with single bonds, C_nH_{2n+2} . Other crucial compounds in the liquid are aromatics and polyaromatics, structured as rings with double bindings.

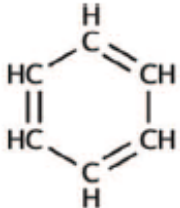
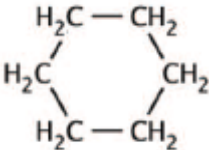
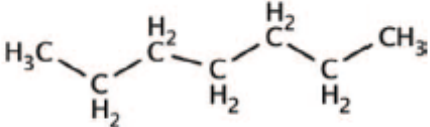
Benzene	Cyclohexane	n-tridecan
		
An aromatic	A naphthenic	An alkane/paraffin

Table 3-1, Nytro 10XN chemical content

Nytro 10XN is a popular transformer oil. It is a suitable cooling agent, good oxidation stability, performs well at low temperatures and has high dielectric strength [22]. The experimental

works initial tests start with this liquid, since previous work have observed rather significant amounts of light emission from this solution, [23].

3.3.2 MIDEL7131

MIDEL 7131 is a synthetic ester-based transformer fluid. Esters are by definition a reaction product from the combination of an acid and alcohol. The chemical structure consist of a carbonyl adjacent to an ether. Hence, the MIDEL 7131 mostly contain single bindings from the ethers, and some double bindings found in the carbonyl [24].

Carbonyl	Ether	Ester
Contain a double bounded oxygen. A & B are arbitrary carbon groups.	Contain an oxygen connected to two alkyl (R) and/or aryl (R') groups.	Combines ether and carbonyl.

Table 3-2, MIDEL 7131 chemical content

MIDEL 7131 has become very popular due to several well performing qualities. It has a long life expectancy, high temperature performance and fire safety. As well as very good moisture tolerance and relative low environmental impact, due to the fact that the liquid is an ester.

3.3.3 Galden HT200

Galden is an inert, fluorinated liquid, largely consisting of perfluoropolyether. The chemical structure of this compound is given as linear single bonded carbon chains with carbon-fluorine bonds and ethers. The fluorine-carbon bond is one the strongest in organic chemistry.

Perfluoropolyether
$\text{CF}_3 - (\text{OCFCF}_2)_n - (\text{OCF}_2)_m - \text{OCF}_3$

Table 3-3, Galden HT200 chemical content

Galden is a liquid dielectric used in several electronics applications. It has a boiling point ranging from 57°C - 270°C, depending on which series applied. The Galden HT200 boils at 200°C. The liquid has good dielectric properties and is an excellent cooling agent. [25]

3.3.4 EXXSOL D80

EXXSOL D80 is a liquid chemical aliphatic hydrocarbon solvent. Its major components are normal paraffin, isoparaffin and cycloparaffin, with a small concentration of aromatic hydrocarbons, <2%. [26]

This liquid is not commonly used as a dielectric, but as a solvent. Utilized in paints, printing inks agricultural use and other applications. Due to complications during testing, this liquid is more or less phased out of this thesis.

3.4 Test Procedure

The test procedure used to extract the wanted data is described here:

1. Changing Liquid

Empty the initial liquid from the test-cell. Fill a small amount of the test solution into the test-cell (≈ 2 dl). Shake and empty the test-cell, in order to clean its inside. Repeat this “cleaning” process 2-3 times, to achieve neglectable concentration of the previous liquid. Fill the whole inside of the test-cell with new liquid (≈ 1.6 l), and close. Avoid air bubbles inside the test-cell.

2. Install the test cell

Mount the test cell inside the Faraday-cage, illustrated in Figure 3.1. Align the test-cell windows with the PMT inside the cage. Connect both sides of the test-cell to its designated points. In this setup, the current-reducing resistance R must be removed in order to free the test-cell from the test-circuit. Semiconductive tape is used to smooth out the coupling surface at R , in order to minimize potential corona during testing. The tape is removed and reapplied with each freeing/installation of the test cell.

3. Start-up

Close the Faraday-cage and fasten the custom grounding system for the circuit. Turn on all apparatus, including signal generator, ICM System, Oscilloscope, Mackie power amplifier, PMT DC supply and laptop. Make sure that all settings are correct and adjust the proper trigger function in the oscilloscope. Calibrate the ICM system with a calibrator, and compare calibration signal on the oscilloscope.

4. Measurements

Start acquisition mode on the ICM System, while simultaneously register single trigger events on the oscilloscope. Register peak amplitude of electrical and PMT-signals on the oscilloscope, where these signals coincide. Additionally register the instantaneous HVAC signal. Register >20 measurements to ensure a solid database. Repeat for all liquids.

3.5 Practical Considerations

Some practical aspects regarding the test setup is discussed here:

Grounding

A custom grounding system for the Faraday cage is constructed. This makes it possible to operate the high voltage test setup alone, while ensuring proper safety considerations for the user. A hollow brass electrode, depicted in Figure 3.6, is placed in top of the HV transformer, T_2 . Point A is the connection to T_2 . The hollow brass cylinder, marked B, can slide into the electrode. A copper “rope” is fitted into the cylinder B. The copper rope is connected to the walls of the Faraday cage, effectively grounding the HV system when point B is inserted into the electrode configuration. A nylon rope is drawn straight through cylinder B and the rest of the configuration. The nylon rope exits the Faraday cage through two drilled holes in cage walls. A 6 kg weight is fastened to one side of the rope, while the other side can be fastened to a hook.

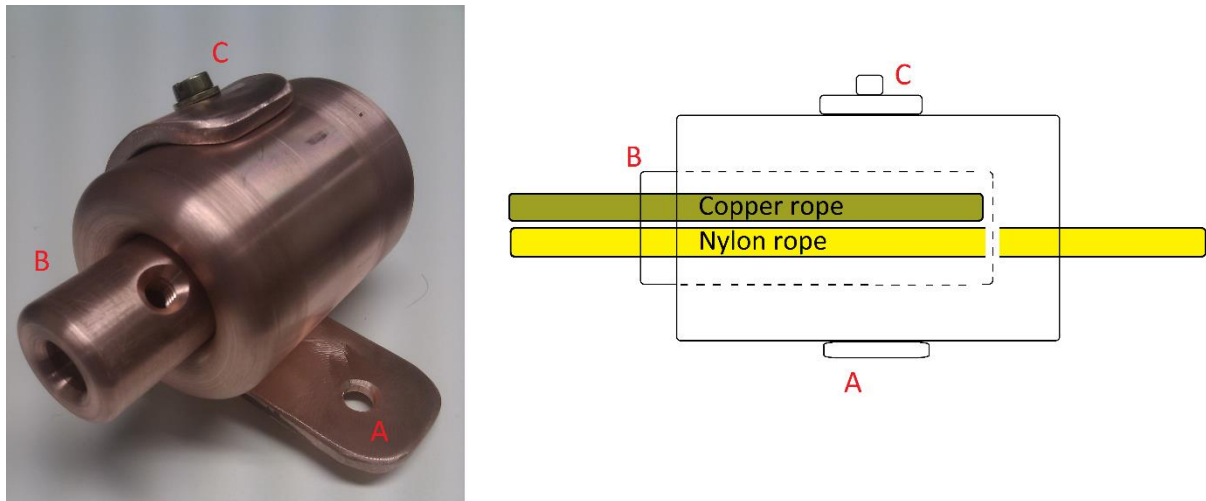


Figure 3.6, HV Brass Electrode

When the Faraday cage door is open, the nylon rope is not fastened at the hook-side. Hence, the weight drags cylinder B into the electrode, and grounds the system. When the cage door is closed, the nylon rope is dragged in front of the door and mounted to a hook. This removes the grounding from the high voltage transformer, and allows for an extra safety mechanism for the Faraday cage.

Cooling

No fitting inductor L_r are readily available at NTNU during the experimental work. A reel of copper wire (6mm diameter X 100m) is used as inductor instead. However, the current passing through L_r heats up the wire. During long tests, the accumulated heat can compromise the insulation of the wire, starting to deteriorate it. An external thermometer and fan is used, to monitor and cool the inductor.

Corona

Sharp edges and narrow points at the high voltage side of the circuit are exposed to develop corona. Corona is an unwanted effect in the circuit, introducing noise and can contaminate

the measurements. Semiconductive tape is used to smooth out all such surfaces at the HV part of the system.

Coupling Capacitor

A coupling capacitor, $\approx 1\text{nF}$, is used at the HV part of the system. Due to the confined space inside the Faraday cage, a custom electrode configuration is constructed to ensure a proper coupling and reduced noise, depicted in Figure 3.7. Two 2nF capacitors in series make up total capacitance. Each capacitor is tested to be PD free up to 20kV .

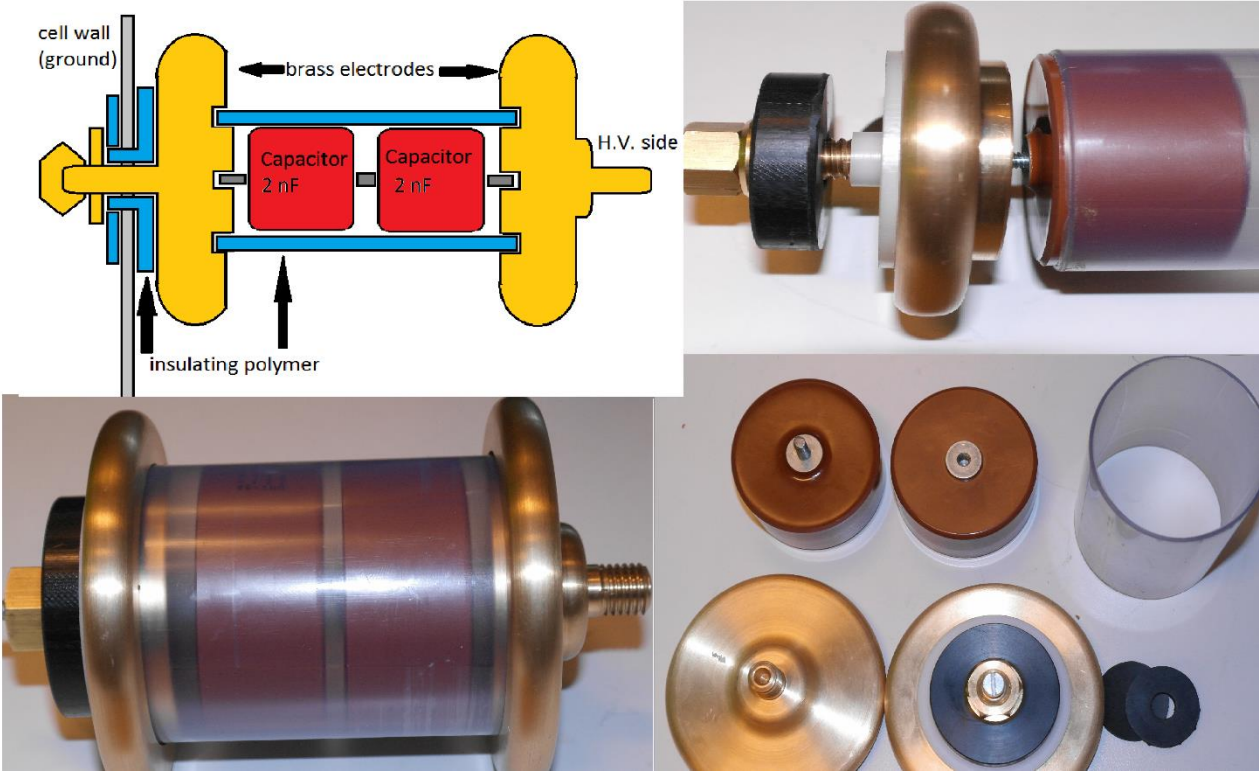


Figure 3.7, Coupling capacitor configuration

4. Results

This chapter presents important calculations, collected data and results leading up to and including the experimental work done for this thesis.

4.1 Circuit Resonance

The test circuit is designed to be able to operate at resonance conditions under several frequencies. However, all measurements are performed with a 50Hz AC signal, due to limited available time.

4.1.1 Model and Simulations

The MATLAB Simulink model gives an indication on the general behaviour of the test circuit and helps determine the appropriate value range for the balancing impedance, L_r . The final model, displayed in Appendix A, has the following components and parameters:

- Z_{eq1-3} : Impedance measurement
- R_{z1-3} : 10^{10} [Ω], impedance measurement parallel resistance
- T_1 : Coupling 40:220, $R_k=0.01$ [Ω], $L_k=0$, $R_m=110$ [Ω], $L_m=0.15$ [H]
- T_2 : Coupling 220:50 000, $R_k=0.38$ [Ω], $L_k=0.53$ [mH], $R_m=830$ [Ω], $L_m=0.406$ [H]
- L_r : 0-20 [mH]
- R_r : 0.3 [Ω]
- C_k : 1023 [pF]
- C_t : 0.1 [pF]
- R_t : 35 [k Ω]

Two simulation scenarios are presented here. Thevenin impedance behaviour vs. frequency, without and with balancing inductance L_r .

Scenario 1, no L_r .

Commenting L_r out of the model display the initial unbalanced test setup. An *impedance vs. frequency* analysis in MATLAB, illustrate the circuit behaviour. The plot also display the phase angle of Z_{th} . Figure 4.1 contain a f vs. Z_{th}/θ plot, with $f \in [0-5\text{kHz}]$:

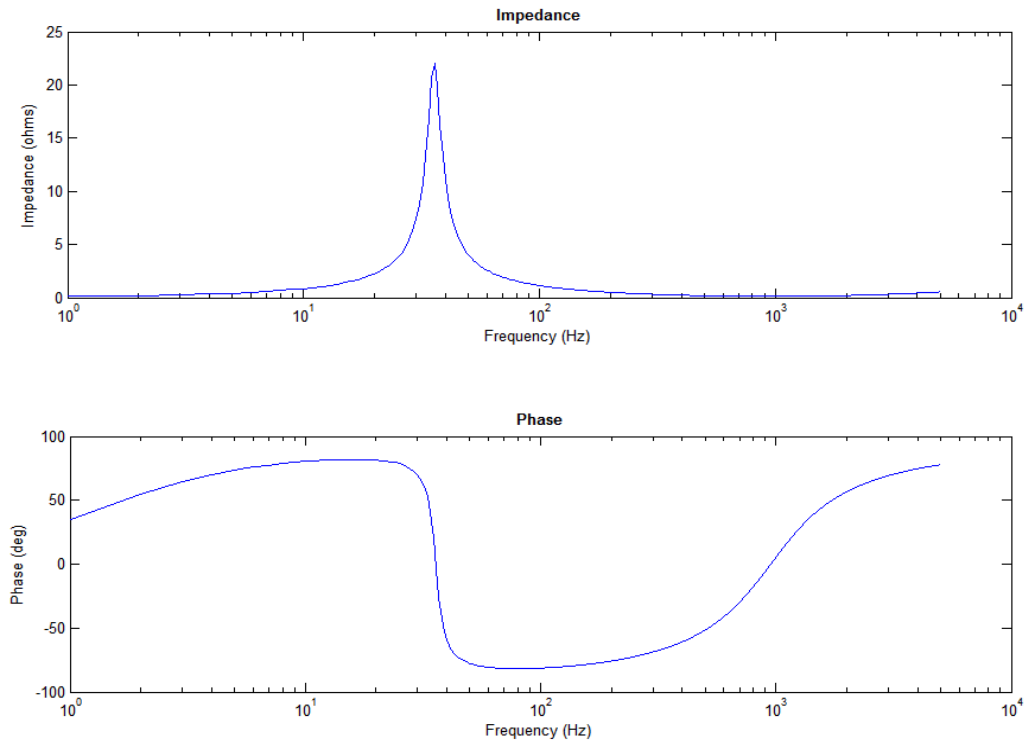


Figure 4.1, f vs. Z_{th} without L_r

$\theta = 0^\circ$ crossing occur at $\approx 35.5\text{Hz}$, with peak impedance $\approx 22.2\Omega$. At 50Hz the Z_{th} impedance is capacitive, $\theta = -77.8^\circ$ and $|Z_{th}| = 4.05\Omega$. Hence, an inductor must be inserted to balance the circuit.

Scenario 2, with L_r

Figure 4.2 depicts a f vs. Z_{th} plot, with $L_r=13.4\text{mH}$ and $f \in [0-5\text{kHz}]$:

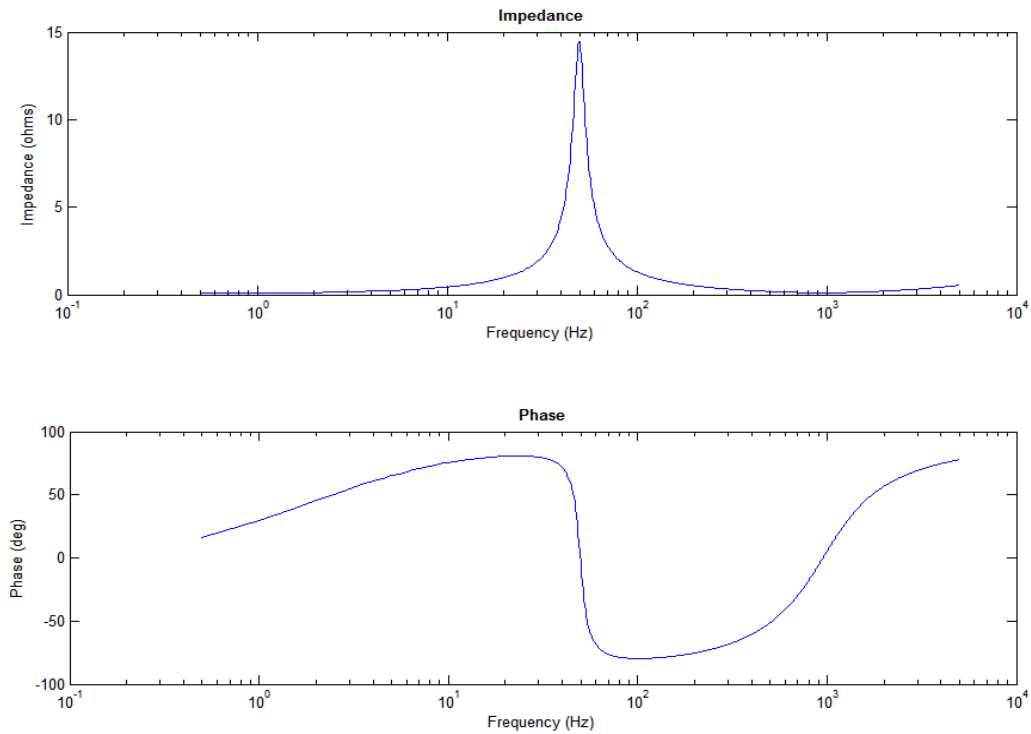


Figure 4.2, f vs. Z_{th} with $L_r=13.4\text{mH}$

This is close to perfect resonance conditions at 50Hz. $\theta \approx 0^\circ$, $Z_{th,max} \approx 14.45\Omega$. Results will be further commented on in the following section.

4.1.2 Experimental Test Circuit Calculations

Several iterations and re-evaluations of the test setup are performed, before the final version is determined, ref. Figure 3.1. Before inserting a balancing component, initial circuit measurements are carried out. These measurements help determine the behaviour of the circuit. The unbalanced test setup is illustrated in Figure 4.3.

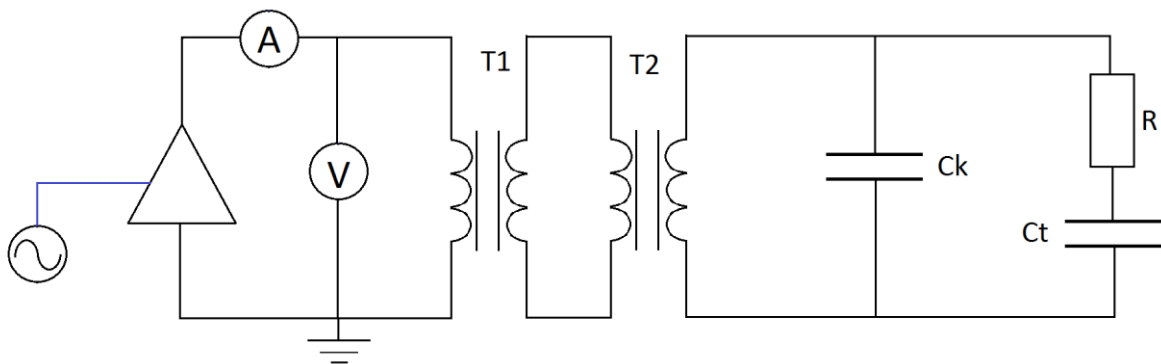


Figure 4.3, Test setup without balancing impedance

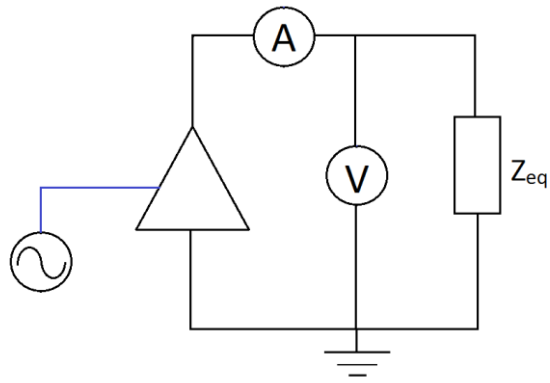


Figure 4.4, Simplified circuit

V	I [A]	P[W]	Q[VAr]	S[VA]	PF
10.4	8.43	21.2	-85.1	87.7	0.24

Table 4-1, Measurements

$$|Z_{eq}| = \frac{V}{I} \quad \text{Eq. 17}$$

$$\theta = \cos^{-1} (PF) \quad \text{Eq. 18}$$

$$Z_{eq} = 1.234e^{-j76.01} \quad \text{Eq. 19}$$

The circuit is clearly capacitive. Hence, a balancing inductor L_r is inserted into the test setup on order to make the circuit purely ohmic.

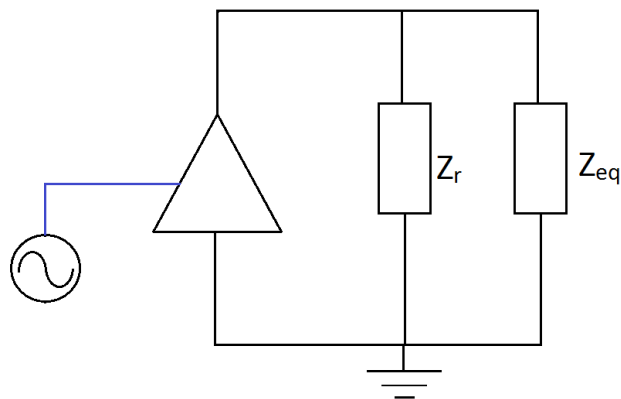


Figure 4.5, Balanced circuit

Ideally the L_r is purely inductive $Z_r = X_r$, with no parasitic resistance. Hence, resonance is achieved when the Thevenin equivalent seen from the amplifier is:

$$Z_{th} = Z_{eq} || Z_r = R_{th} \quad \text{Eq. 20}$$

Inserting values from Eq. 19 and assuming $Z_r = X_r$, gives:

$$Z_{th} = \frac{1.234e^{-j76.01} * X_r e^{j90}}{1.234e^{-j76.01} + X_r e^{j90}} \quad \text{Eq. 21}$$

Wanting to achieve $\theta_{th}=0^\circ$, Eq. 21 can be manipulated to find the correct value for X_r .

$$\tan^{-1} \left(\frac{X_r - 1.2}{0.298} \right) = 13.99 \quad \text{Eq. 22}$$

$$X_r = 1.274 \quad \text{Eq. 23}$$

At 50Hz, this makes:

$$L_r = 4.06 \text{ mH} \quad \text{Eq. 24}$$

However, limited assortment of inductors leads L_r to be less ideal. As mentioned in section 3.5 Practical Considerations, a 6mmX100m copper wire is used as L_r . By adjusting the amount of wire lashed on the wire barrel, the inductance of L_r can be alternated. The wire resistance is measured to be 0.3Ω , while L can be varied between 0-4mH. L_r has been set to 3.52mH for all PD measurements performed in this experimental work.

$$Z_r = 0.3 + j1.106 \quad \text{Eq. 25}$$

$$Z_{th} = Z_r || Z_{eq} \quad \text{Eq. 26}$$

$$\begin{aligned} Z_{th} &= 2.34e^{j7.8} \\ &= 2.3 + j0.32 \end{aligned} \quad \text{Eq. 27}$$

This Thevenin equivalent is sufficiently close to resonance conditions.

4.2 Electrical Field

The tip of the tungsten wire on the point electrode is measured using a microscope connected to a computer. The radius of curvature is measured to be $20\mu\text{m}$, with an uncertainty of $\approx 0.5\mu\text{m}$. The gap distance between the point-plane electrodes is set to be 20mm , with about $\approx 0.5\text{mm}$ uncertainty.

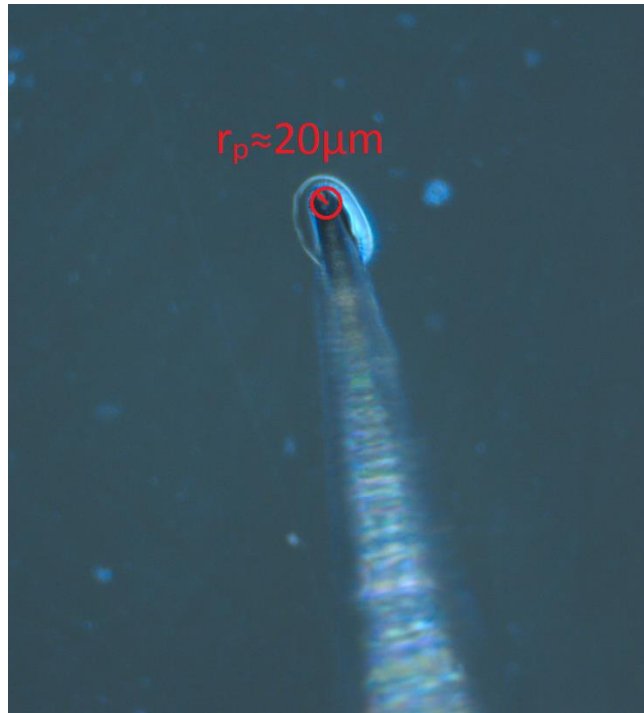


Figure 4.6, Tungsten wire tip, r_p

The electrical field directly perpendicular to the wire tip is estimated by Eq. 7:

$$E_{tip} = \frac{2V}{20 * 10^{-6} \ln\left(\frac{4 * 20 * 10^{-3}}{20 * 10^{-6}}\right)} \quad \text{Eq. 28}$$

Varying the applied AC voltage by $15\text{-}28\text{ kV,rms}$ gives $E_{tip} \in [0\text{-}477]$ [MV/m]. This field strength is more than sufficient to initiate both small negative and large positive PDs in the liquid bulk.

4.3 PD Measurements

Inverted Signal Measurements!

The ICM System usually measures PD activity by the means of a quadrupole connected in series with coupling capacitors. In the setup used here, the measurements are performed in series with the test cell. Hence, all voltage signals and PD activity are inverted by the test setup. The negative half period of the HVAC, displayed on the ICM system and the oscilloscope is in reality the positive part, and vice versa for the positive half period. All collected data is displayed here in their original (inverted) form, if not otherwise stated.

The PMT output signal is always negative, regardless of the polarity of the PD. This is because of the photocathode-anode configuration, outputting negative electron signals. Nevertheless, the 2/4/6 preamp used to amplify the PMT output inverts the signal. Displaying all light signals on the oscilloscope as positive polarity.

The oscilloscope registers three signal inputs during PD test:

- CH1: PMT signal. Inverted, integrated and amplified 20/40dB, yellow colour
- CH2: Electrical PD pulse. Inverted, integrated and amplified 0/20dB, blue colour
- CH3: HVAC. Reduced by X 1/1000, purple colour

All collected data from the oscilloscope is displayed in Appendix C.

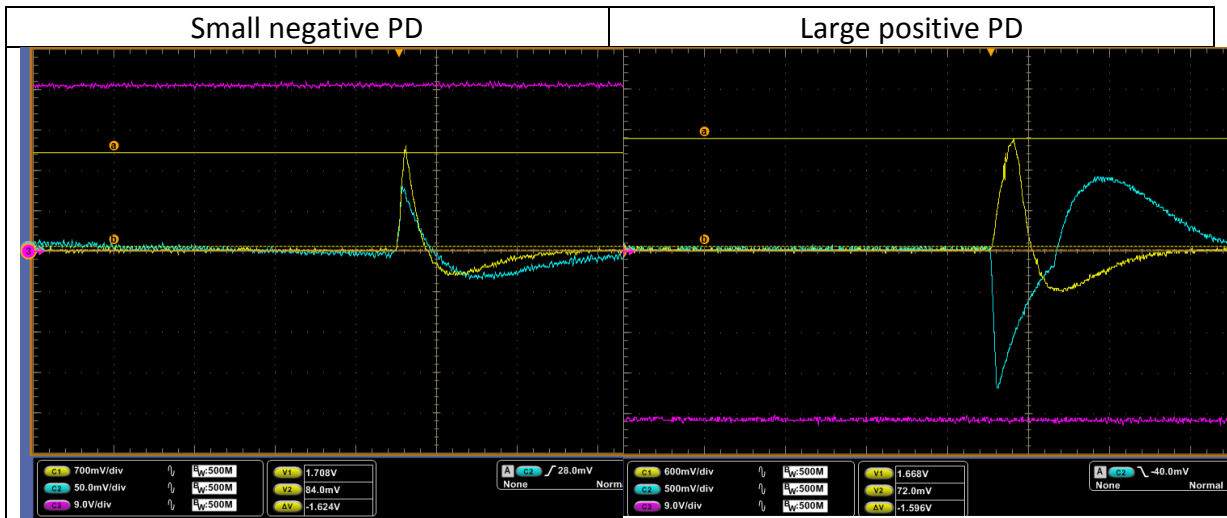


Table 4-2, Typical single PD signal from oscilloscope. (left) negative PD, (right) positive PD. Both taken from Nytro 10XN measurements. Note that ALL signals displayed here are originally inverted!

In order to achieve sufficient light measurements for the small negative PD streamers, the PMT is supplied near its max voltage limit, 1500V DC. However, large positive PDs emit generally much more light than their small negative counterparts. Hence, the PMT output signal is much larger for positive PDs compared to the negative ones. In some cases the CH1 light signal experiences a saturation limit. Producing the same signal strength for all positive signals (approx. 3000mV). This saturation is restricted either by the max output of the PMT or max output by the 2/4/6 preamp. Therefore it is decided that the PMT supply voltage is alternated, regarding which PD phenomenon is studied.

PD type	V _{PMT} Supply [V]	Current amplification
Large positive streamer	600	≈1.5*10 ⁴
Small negative streamer	1480	≈2.6*10 ⁶

Table 4-3, PMT supply vs gain

The different output signals are found using the gain characteristics for the R1635 PMT, seen in Figure 3.5.

4.3.1 Nytro 10XN

Water content

Average water content, pr. 2 ml sample	Density	Total water content
20.37[μg]	872 [kg/m^3]	11.68 [ppm]

Table 4-4, Nytro 10XN water measurement

Negative PD

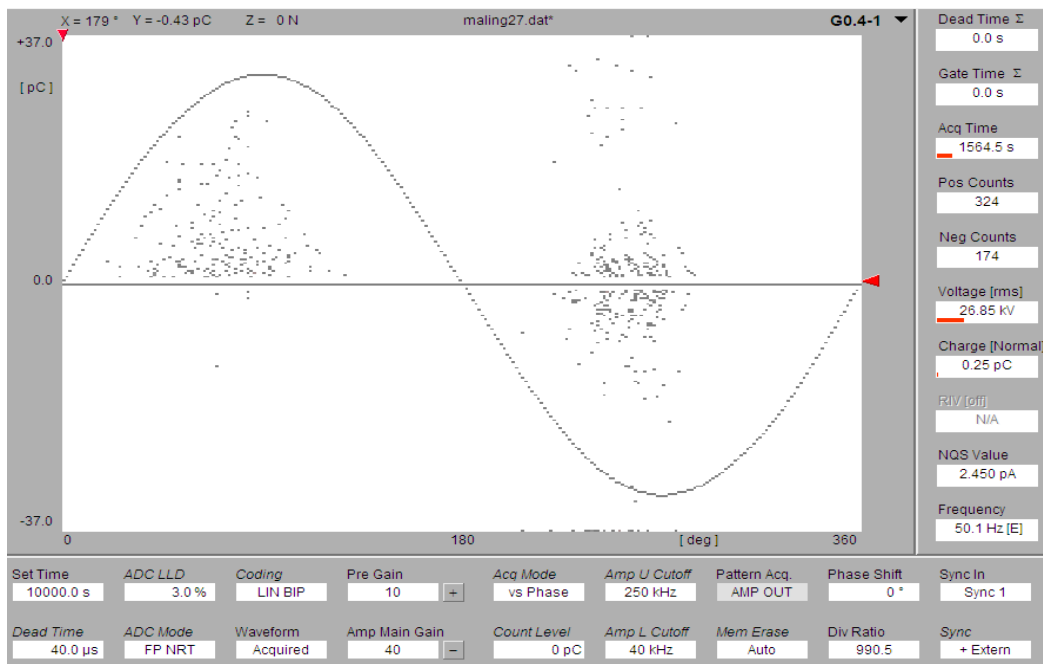


Figure 4.7, Nytro 10XN ICM small negative PD pattern

Figure 4.7 depict the ICM system plot, during small negative PDs. Pre gain is set to 10=20dB. Note the large negative PDs at positive half period (right hand side) is most likely caused by the previous large positive discharge, causing oscillation.

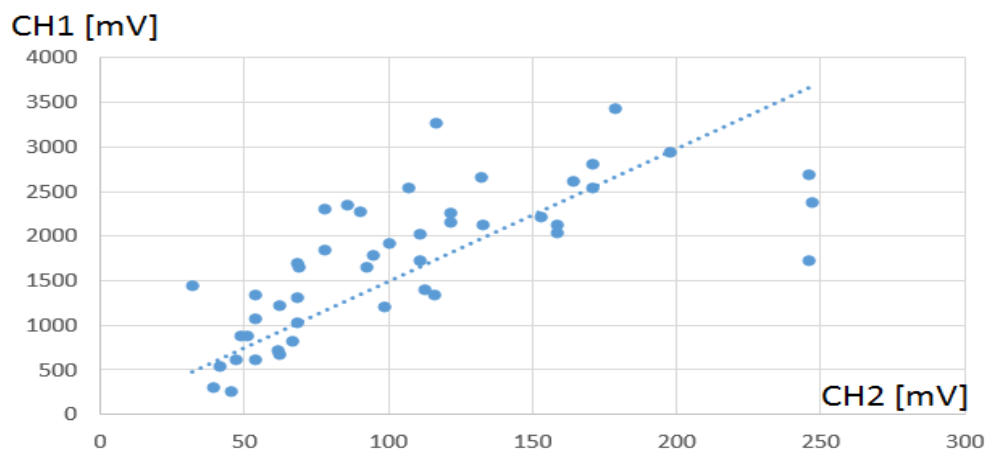


Figure 4.8, Nytro 10XN negative PD plot

Figure 4.8 display the light measurements (CH1) vs. the electrical PD measurements (CH2). CH1 2/4/6 amplifier is set to 40dB, and $V_{PMT\ Supply} = 1480V\ DC$.

Positive PD

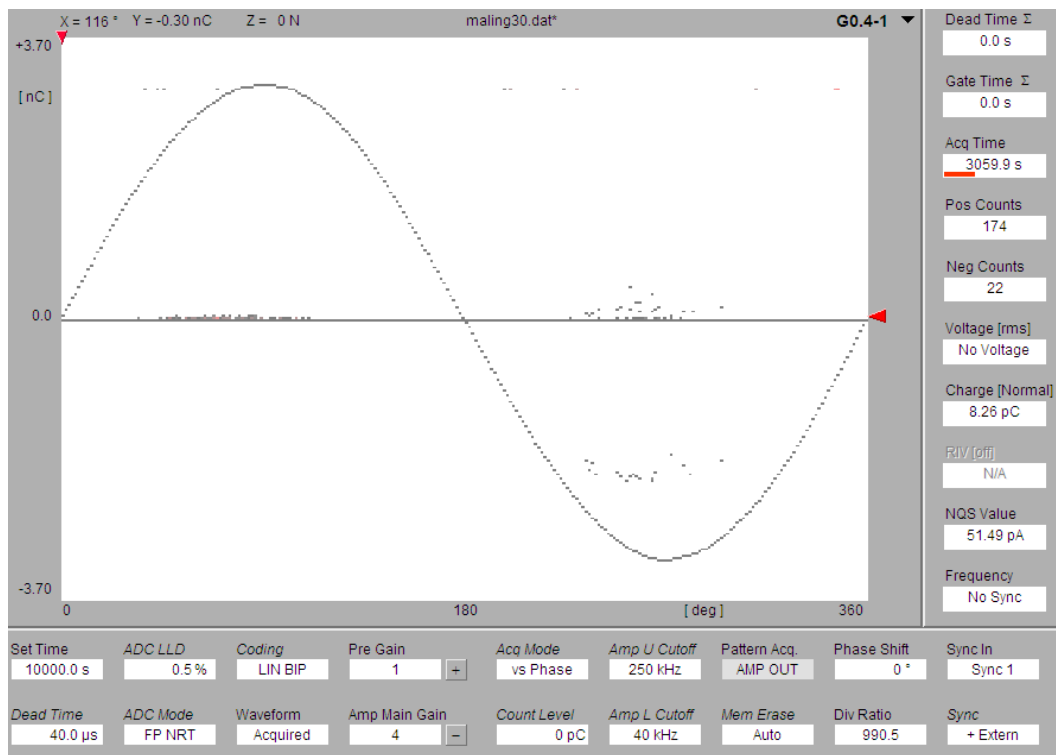


Figure 4.9, Nytro 10XN ICM large positive PD pattern

Figure 4.9 depict the ICM plot during large positive PDs in Nytro 10XN. Pre amp is set to 1=0dB.

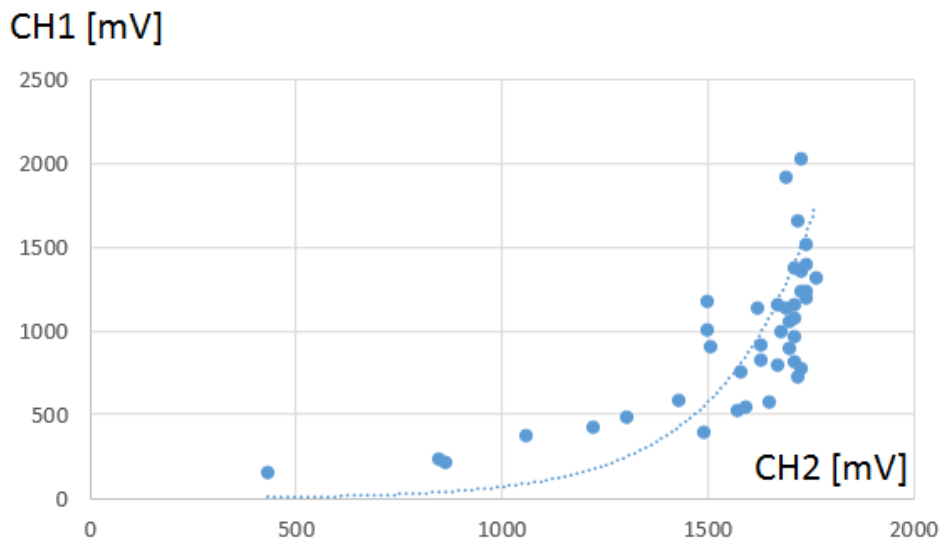


Figure 4.10, Nytro 10XN positive PD. CH2 inverted

Figure 4.10 depict light measurement (CH1) vs. electrical PD signals (CH2) for large positive PDs in Nytro 10XN. CH1 2/4/6 amplifier is set to 40dB, and $V_{PMT\ Supply} = 600V\ DC$. Note different measures of light emission at the same approx. PD magnitude.

4.3.2 MIDEL 7131

Water content

Average water content, pr. 2 ml sample	Density	Total water content
49.85[μg]	970[kg/m^3]	25.7 [ppm]

Table 4-5, MIDEL 7131 water measurement

Negative PD

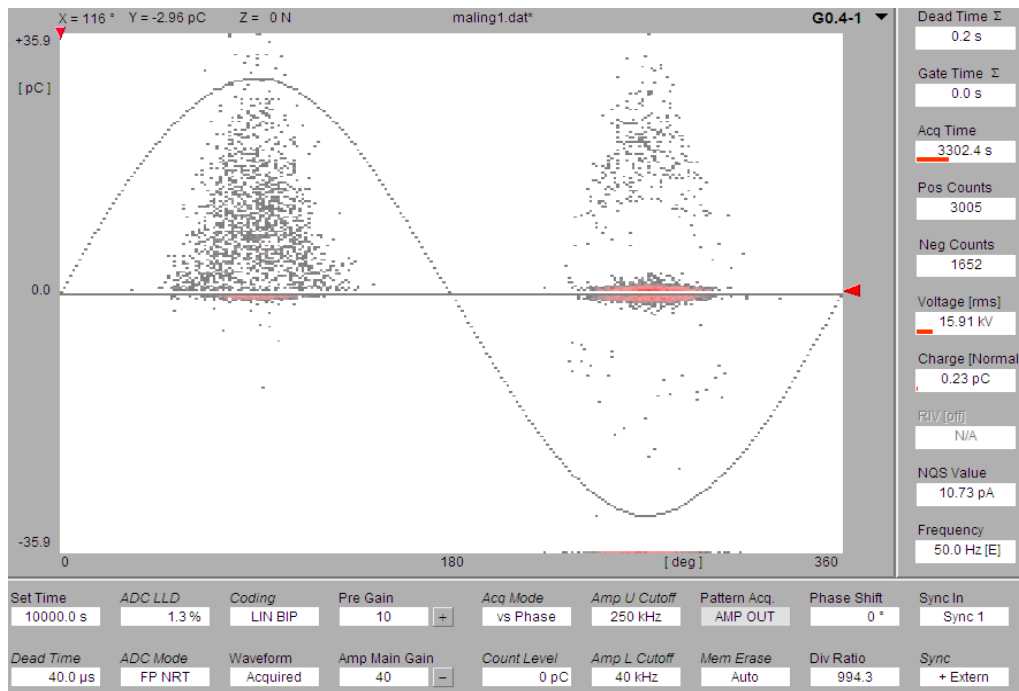


Figure 4.11, MIDEL 7131 ICM small negative PD pattern

Figure 4.11 depict the ICM system plot, during small negative PDs. Pre gain is set to 10=20dB.

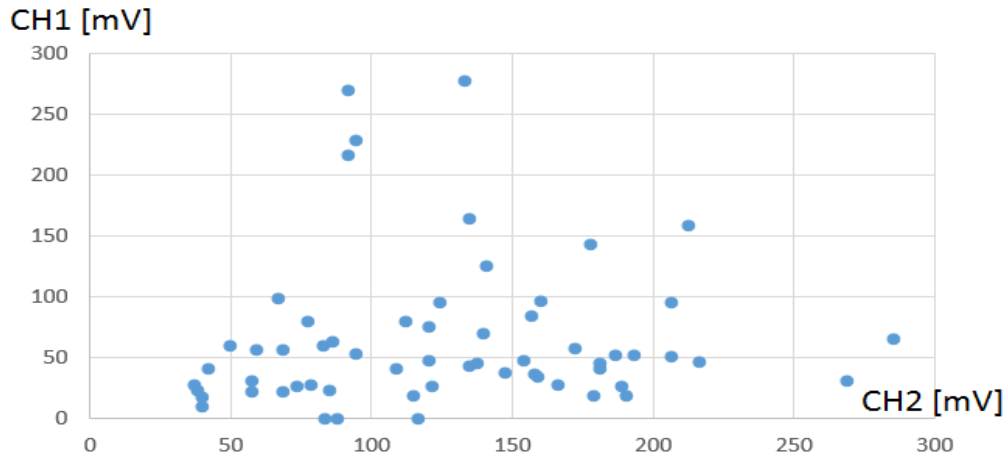


Figure 4.12, MIDEL 7131 negative PD plot

Figure 4.12 display the light measurements (CH1) vs. the electrical PD measurements (CH2). CH1 2/4/6 amplifier is set to 40dB, and $V_{PMT\ Supply} = 1480V\ DC$. Note scatter in the plot.

Positive PD

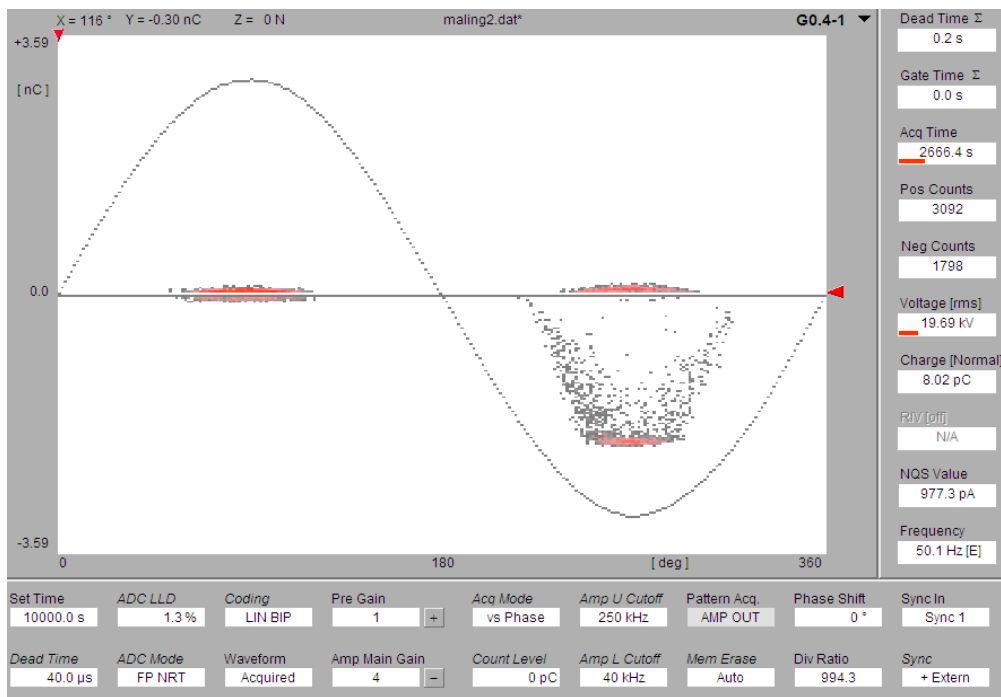


Figure 4.13, MIDEL 7131 ICM large positive PD pattern

Figure 4.13 depict the ICM plot during large positive PDs in MIDEL 7131. Pre amp is set to 1=0dB.

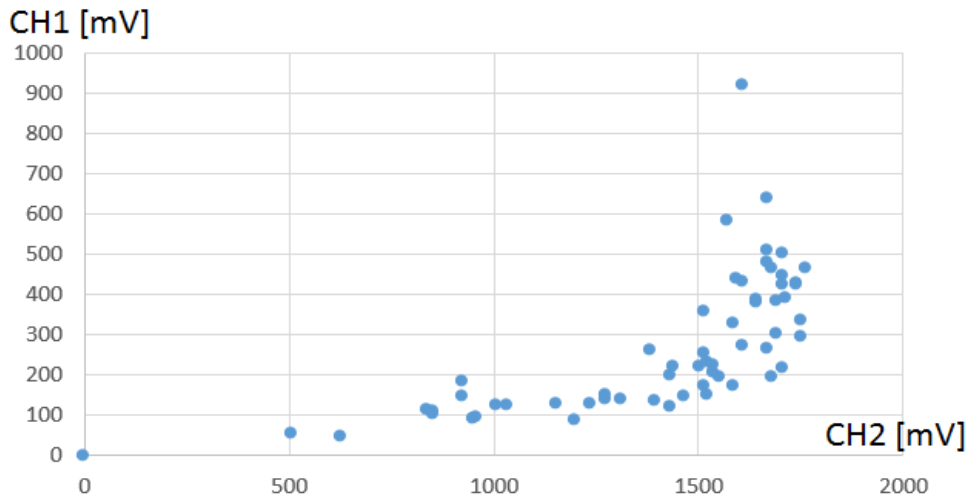


Figure 4.14, MIDEL 7131 positive PD plot. CH2 inverted for illustrative reasons.

Figure 4.14 depict light measurement (CH1) vs. electrical PD signals (CH2) for large positive PDs in MIDEL 7131. CH1 2/4/6 amplifier is set to 40dB, and $V_{PMT\ Supply} = 600V\ DC$. Similar tendency as for Nytro 10XN.

4.3.3 Galden HT200

Water content

Did not measure water content due to the belief that Hydranal-solution not being capable of handling the Galden HT200 fluid during a Karl-Fisher test.

Negative PD

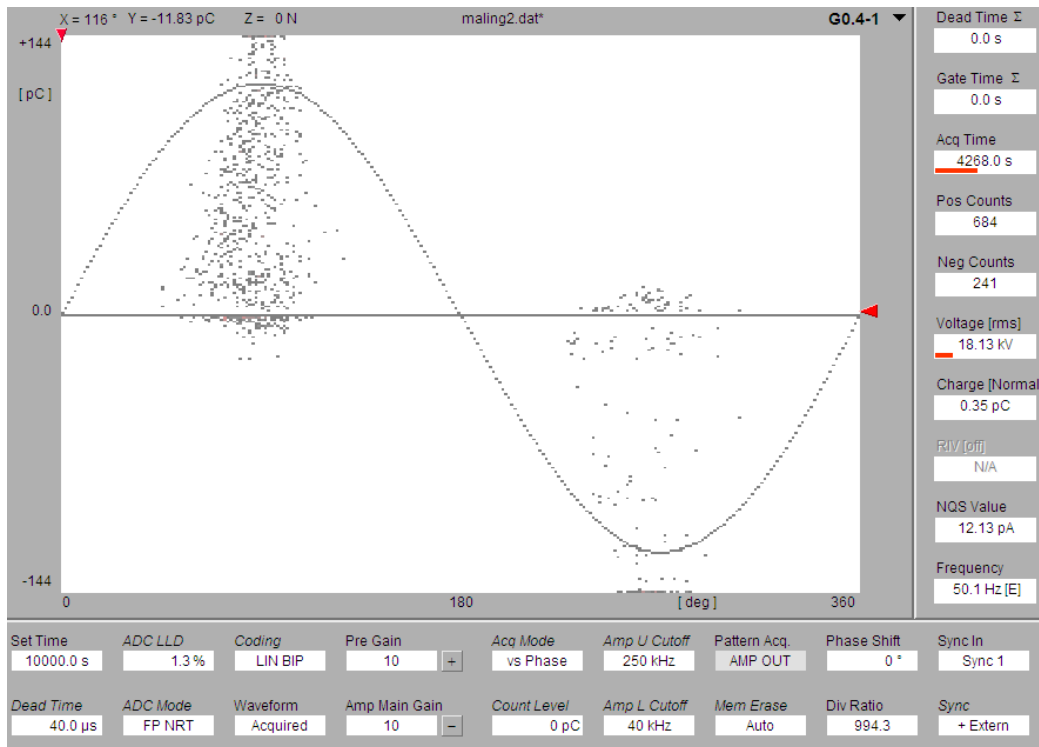


Figure 4.15, Galden HT200 ICM small negative PD pattern

Figure 4.15 depict the ICM system plot, during small negative PDs. Pre gain is set to 10=20dB. Note the magnitude of the “small” negative PDs.

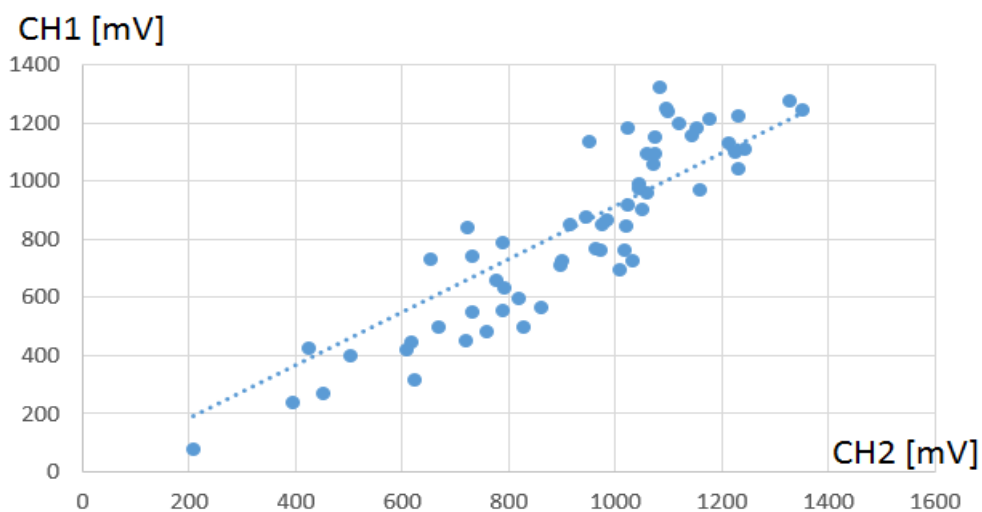


Figure 4.16, Galden HT200 negative PD plot

Figure 4.16 display the light measurements (CH1) vs. the electrical PD measurements (CH2). NOTE: CH1 2/4/6 amplifier is set to 20dB, due to saturation conditions. $V_{PMT\ Supply} = 1480V\ DC$.

Positive PD

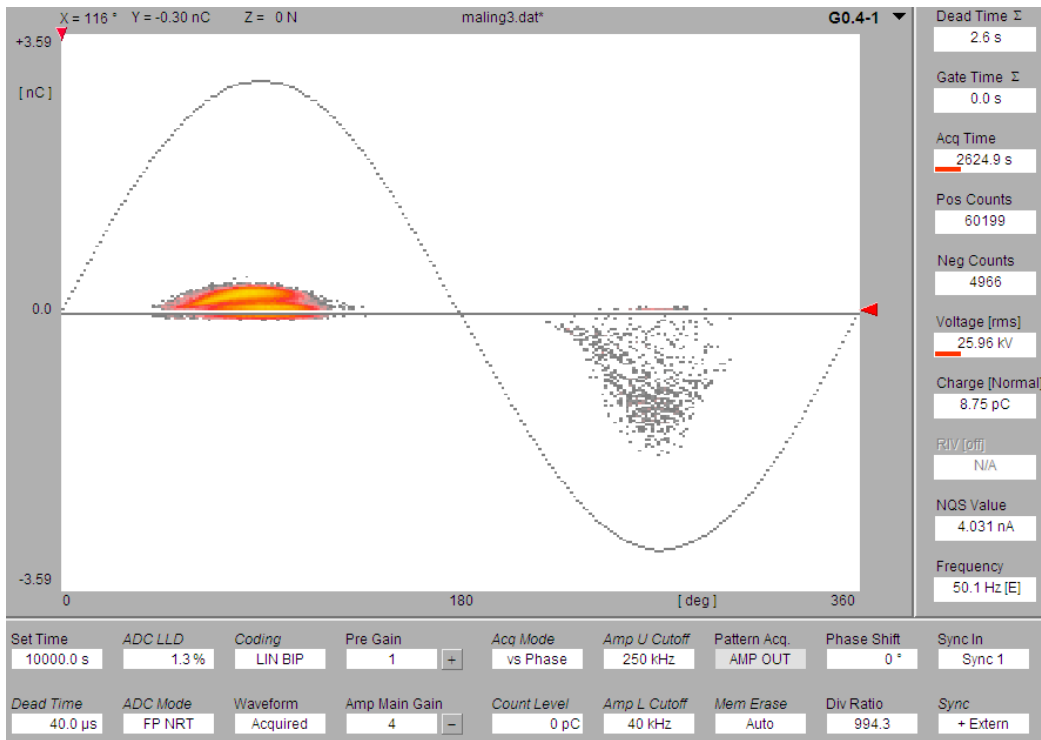


Figure 4.17, Galden HT200 ICM large positive PD pattern

Figure 4.17 depict the ICM plot during large positive PDs in MIDEL 7131. Pre amp is set to 1=0dB. Note the vast amount of relative large negative discharges in this period.

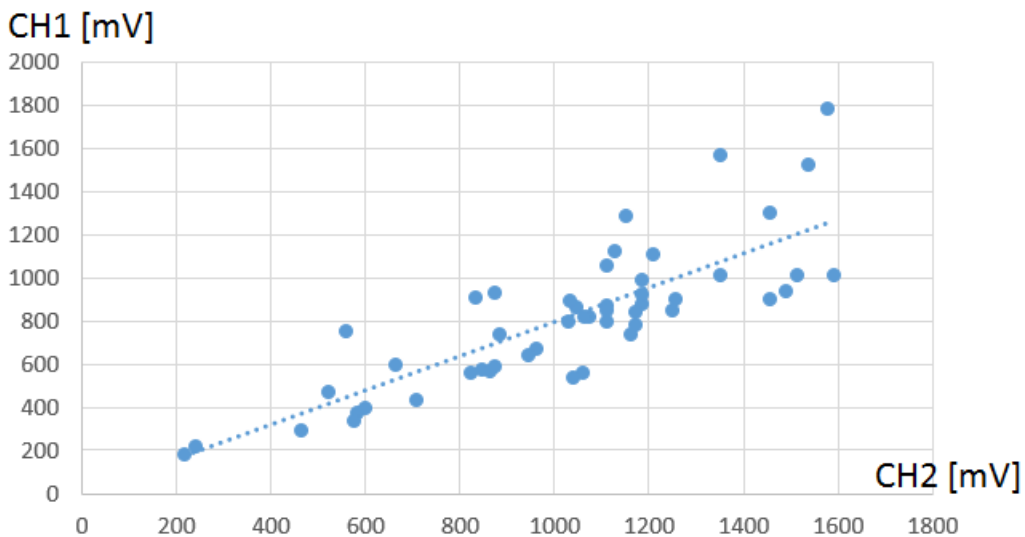


Figure 4.18, Galden HT200 positive PD plot. CH2 inverted for illustrative reasons.

Figure 4.18 depict light measurement (CH1) vs. electrical PD signals (CH2) for large positive PDs in Galden HT200. CH1 2/4/6 amplifier is set to 40dB, and $V_{PMT\ Supply} = 600V\ DC$.

4.3.4 EXXSOL D80

The utilized test setup have problem initiating sufficient PD activity in the EXXSOL D80 liquid. Even with CH2 preamp set to a gain of 40dB and HVAC supply near 28kV, only sparse PD activity is observed. The small amount of PD activity that is being registered, produce a small PMT signal at CH2 of the oscilloscope. The 2/4/6 CH1 preamp is set to 40dB gain.

The same problems are observed at measurements of large positive PDs. Only that the occurrence of these PDs are even more sparse then for the negative small counterparts. After 200s of applied 29kV,rms only one PD above 200pC is registered. This single PD occur in the opposite half period, than what is being studied.

When trying to increase HVAC above 29kV, in order to force more PD, complete breakdown occur. These complications leads to EXXSOL D80 liquid not capable of producing satisfying data. Hence, EXXSOL D80 is phased out for further discussion and comparison between other dielectric liquids.

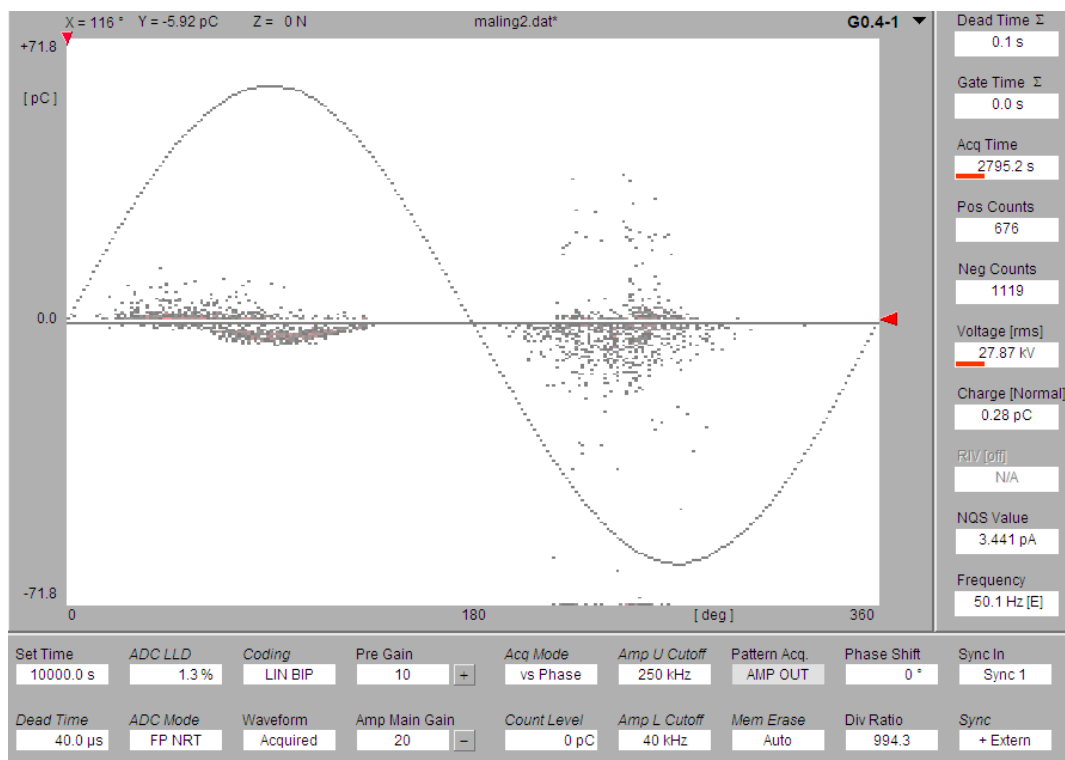


Figure 4.19, EXXSOL D80 ICM plot. Note the inverse polarity of discharges in the negative half period (left part the graph).

4.3.5 Combined PD Plot

Converting all CH2 PD measurements into their respective charge magnitude, given in pC. The conversion is done in regard to each liquids calibration test done pre PD measurements. A combined PD plot for both negative and positive streamers are depicted in Figure 4.20 and Figure 4.21 respectively. Note that the negative *Galden HT200* measurements are performed with 20dB amplification into CH1, while the other PMT signals are amplified by 40dB. Hence, to get comparable results the *Galden* CH1 data is multiplied by a factor of 10.

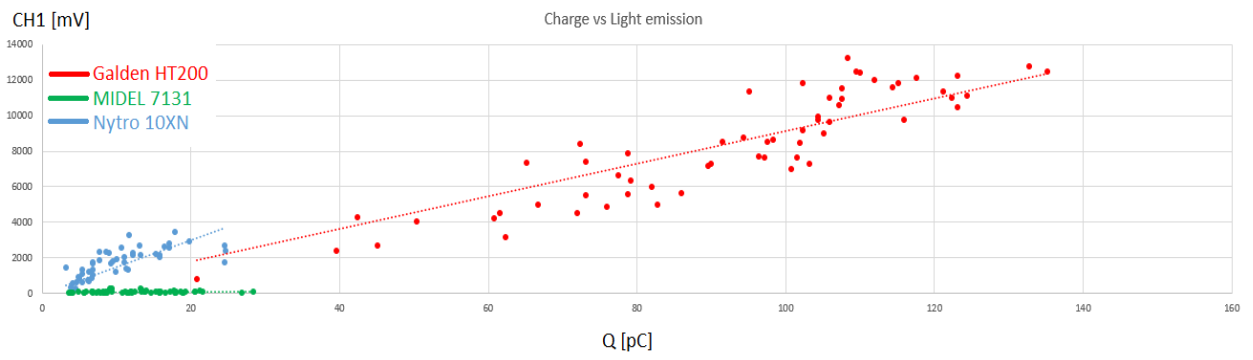


Figure 4.20, Combined negative streamer, Q vs PMT signal. PMT supply voltage =1480V DC.

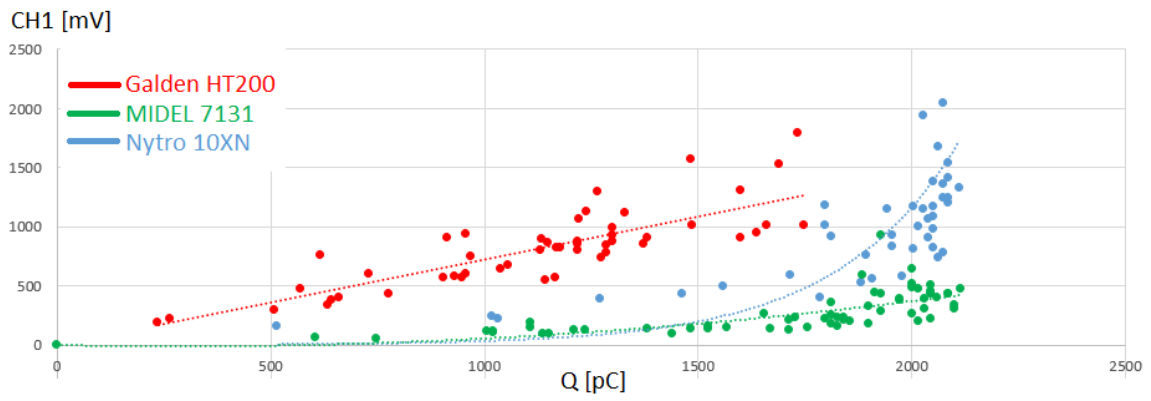


Figure 4.21, Combined positive streamer, Q vs PMT signal. PMT supply voltage =600V DC.

5. Discussion

This chapter comment the results found in the previous chapter, illustrate common trends in the results and display the content of the measured data. First the test setup and Simulink model is discussed, then the PD measurements and their results. Finally, an energy comparison is displayed and discussed.

5.1 Test Circuit

5.1.1 Simulink Model

At 50Hz resonance the *MATLAB Simulink* model calculate $|Z_{th}| = 14.45\Omega$ and $L_r = 13.4\text{mH}$. This is quite different from the actual measured values in the test setup. This difference clearly indicate a flaw in the test model. In the utilized model the series inductance of the two transformers, T_1 and T_2 is set to 0[H] . It is observed that by changing the series impedance only slightly greatly change the behaviour of the model circuit. Other sources of model flaw may be other parasitic elements in the circuit. Such as cable impedance, capacitor resistance and incorrect magnetization resistance/inductance. However, the model is only used as guideline for the test setup, and not as a precise measuring tool. Hence, it is acceptable for it not to behave 100% correct, as long as it gives an indication of the general behaviour.

5.1.2 Test Circuit Behaviour

The test circuit behaves quite satisfying during PD measurements. The setup is nearly noise free, with electrical noise $<0.4\text{ pC}$. Regarding the PD signals are in the order of 2 pC - 3 nC , these conditions are sufficient. Near perfect resonance conditions are achieved when the AC frequency is set to 50Hz. By alternating the balancing impedance L_r from 0 - 4mH , resonance conditions can be achieved for several different frequencies. However, heating of L_r is a problem. When operating at high voltages ($\text{HVAC} > 25\text{kV, rms}$), the inductor becomes warm relative quickly. After approx. 30 minutes the inner windings of the inductor reaches temperatures near 70°C . The tests must then be paused, in order for the windings to cool off.

The total impedance of the system, when operating at $f=50\text{Hz}$ is found to be $|Z_{th}| = 2.34\Omega$. This is a crucial parameter, since the *Mackie M1400 power amplifier* needs to “see” at least 2Ω in order not to operate near short circuit conditions. Overall, the total impedance of the system is on the lower scale of what should be used. If the circuit design is altered, total impedance should be increased, which will lead to a current reduction. Probably removing/reducing the heating problem already mentioned.

5.2 Partial Discharges

5.2.1 PD development

Applied voltage

As observed in Figure 4.7, 4.9, 4.11, 4.13, 4.15 and 4.17 the HVAC supply is not constant for all PD measurements. A couple of conditions govern when applied voltage is chosen for the tests. Firstly, the signal generator in combination with the power amplifier is difficult to control with high sensitivity. Leading to some alternation in the applied voltage between different tests. Second, the different liquids experience different rate of PD activity and PD magnitude at different voltage levels. Since this thesis mainly study light emission from PD activity, and not voltage level vs. PD initiation, some difference in supply voltage is tolerated. Nevertheless, the voltage level of the different PDs in the three liquids are recognized and commented on. See section below for more on this. Generally, a higher supply voltage is used to initiate positive streamers, than negative streamers. Even though some positive streamers are observed for lower voltage ratings, the occurrence is much more consistence and predictable when a stronger electrical field is present. This helps ease the experimental work, by reducing the time needed to collect sufficient data.

Needle tip

The tip of the tungsten wire, used as point electrode is measured to have a radius of curvature $r_p \approx 20 \mu\text{m}$. This radius may change during experiments, due to etching at tip, from the ionized liquids, as well deterioration caused by occurrences of breakdown and PD. As discussed in section 2.2 Point-Plane Geometry, increased r_p greatly affect the electrical field. Previous work [14] have indicated that the tip radii increase rapidly at $2-8 \mu\text{m}$ in the presence of a sufficient electrical field in MIDEAL 7131. When $r_p > 10 \mu\text{m}$ the rate of increase flattens out. Hence, it is possible to suggest that when $r_p \approx 20 \mu\text{m}$ the tip radius will not change dramatically during tests, unless breakdown occur. r_p is not monitored closely during tests in these experiments. As long the setup is capable of initiating sufficient PDs, without causing breakdown and overstress the setup, the tip radii is not a crucial parameter.

EXXSOL D80

The EXXSOL D80 liquid has problems initiating sufficient PD activity during tests. Several factors may complicate the PD measurements for this liquid. It is for instance observed that the EXXSOL D80 test sample is not completely pure. Particles are observed in the fluid. Such particles can affect the PD pattern in the bulk, due to ionization of particles. Further, this is the last liquid being tested. This may be disadvantageous for the liquid experiment, due to previous tests may have dulled the point electrode tip. As discussed, a dull tip will reduce the electrical field, and stall the initiation of PD. Lastly, it may also be the case that the EXXSOL D80 liquid in itself does not have a significant difference between PD and breakdown voltage levels. Nevertheless, it is unfortunate that the EXXSOL D80 liquid is not thoroughly tested.

5.2.2 PD Charge Magnitude Measurements

General PD behaviour

The PDs studied in the thesis consist of small negative streamers at negative half period of the HVAC, and positive streamers in the positive half period. The general trend seen for all liquids, except EXXSOL D80, is a high amount of negative discharges and fewer positive. This is expected regarding section 2.1.1 PD Development in Liquids. The negative streamers are expected to have different governing initiation mechanisms than the positive streamers. A majority of the PDs, for both polarities, appear at the rising edge of the voltage. The electrical field is gradually increased as the AC voltage grows. Observing a surplus of PDs at the rising slope is therefore not surprising, due to the applied frequency “only” being 50Hz. The initiation mechanisms for the PDs have sufficient time to develop during the rise time of the voltage. Hence, PDs will initiate as the HVAC reaches a threshold limit. It is also observed some relative large negative PDs in the positive half period of the three studied liquids, as seen in Figure 4.7, 4.9, 4.11 and 4.15. These PDs are seen to develop directly after the large positive PDs, and may therefore be seen as a phenomenon closely connected to the positive streamers. The origin of these PDs are not studied in this thesis, and is not measured or registered in any data plot.

Nytro 10XN is observed to initiate the least amount of PDs of all the tested liquids. The *Nytro 10XN* liquid is a transformer oil, and is designed to be able to handle high field stress, while keeping its dielectric properties. Figure 4.7 depicts that only 498 PDs are registered, during 1564 seconds of sampling time at HVAC=26kV,rms. 324 of these PDs have negative polarity. Thus, the negative PD rate is ≈ 0.2 [-PD/s]. The positive PDs in the *Nytro 10XN* liquid are fairly large $>1\text{nC}$.

MIDEL 7131 is the tested liquid that initiates the largest amount of PDs. PD activity is observed at much lower voltage levels, than the two other liquids, and with a much higher rate of development. Seen in Figure 4.11, 4657 PDs are registered during a sampling time of 3302 seconds, of which 3005 are negative PDs. Negative PD rate is then 0.91 [-PD/s] at HVAC $\approx 16\text{kV,rms}$. Even though the rate of PDs is large in the *MIDEL 7131* liquid, the size of PDs are not particularly large. It can be noted that the PD measurements for this liquid perhaps have been misguided by the sheer amount of PD activity. Meaning that the voltage level is set too low during tests. The combined PD plot for negative PDs seen in Figure 4.20 might have been different for the *MIDEL 7131* liquid (green dots) if the applied supply voltage had been greater. As for positive streamers, *MIDEL 7131* is observed to produce similar results as *Nytro* and *Galden*. Here the HVAC supply is also of a lower magnitude than the two other liquids.

Galden HT200 initiates a PD pattern quite similar to that of *Nytro 10XN*, just at lower applied HVAC. The negative streamers are in general of a larger magnitude than those of *Nytro* and *MIDEL*, and are produced at an initiation rate of ≈ 0.22 [-PD/s] at HVAC=18.1kV,rms. As for positive streamers, the *Galden HT200* liquid initiates PDs in the range 0.2 - 1.6nC at HVAC=26kV,rms, seen in Figure 4.17 and 4.18.

Possible measurement errors

The RPA1, preamplifier used in the ICM measurements will have a small gain flaw, hence not amplifying the signal 100% accurate to its gain specifications. Further, the oscilloscope has a

specified sampling speed and a fixed number of possible data plots in its display window. This makes the oscilloscope measurements contain some variance.

5.2.3 Light Emission

PMT signals

By studying Figure 4.20 and Figure 4.21, it may seem like the small negative streamers produce more light than the positive streamers. This is however not the case, as displayed in Table 4-3. The two different PD phenomenon utilize two different supply voltage levels for the PMT. In order to achieve comparable light measurements between negative and positive streamers, the gain difference in the PMT output signal must be accounted for. The gain difference is, given by Table 4-3:

$$\begin{aligned}\Delta PMT gain &= \frac{2.6 * 10^6}{1.5 * 10^4} && Eq. 29 \\ &= 173.3\end{aligned}$$

Multiplying all positive CH1 light measurements by a factor of ≈ 173.3 , comparable light data is obtained between the two PD phenomenon. It now becomes clear that the general positive streamers emit much more light than the negative ones.

The *R1635* PMT output signal is given in ampere per lumen [A/lm]. However, the exact amount of light emitted by the PDs is not calculated here. The placement of the PMT allows only a fraction of the photons in the PDs to reach the photocathode. This makes the test setup not suitable to measure the correct lumen activity. Further, the PMT part of the circuit contain both a signal integrator and a voltage amplifier. These components make it impractical to calculate the light activity at the photocathode, and would most likely lead to an incorrect calculation. The important aspect of the light emission measurements in this thesis is to study the relative light signal difference between different PD magnitudes for positive and negative PD streamers, for the different liquids.

Possible measurement errors

It is important to understand the limitations of the utilized test setup, in order to comprehend the collected data from the experimental work. As mentioned the total amount of light from PDs are not registered by the PMT. The modified *R1635 PMT* has a different spectral response then the original tube. The different PMT gains used in the test setup is not completely accurate. The gain levels are read out of Figure 3.5, and may be somewhat misread.

5.2.4 Light Measurement vs. Electrical PD Pulse

Negative Streamers

Figure 4.20 depict the combined plot of PD magnitude vs light emission for negative streamers in the three measured liquids. It is clearly seen that the amount of light is very different for

each liquid. Both Nytro 10XN and Galden HT200 seem to display a clear connection between the magnitude of the negative PDs, and the amount of photon activity in the liquid. The relation between the two data can be estimated as a linear band, and is graphed in Figure 4.20. Galden HT200 has a larger magnitude on the PDs and more light activity than the Nytro 10XN. The negative streamers in MIDEEL 7131 is observed to be more or less stochastic, with no clear correlation between PD magnitude and light emission.

Positive Streamers

Figure 4.21 depict the combined plot of PD magnitude vs light emission for positive streamers in the three measured liquids. A strong correlation between light emission and PD magnitude is observed for all three liquids. According to these measurements, Galden HT200 seems to emit the most light per charge in the PD streamer. Both the Galden HT200 and the MIDEEL 7131 is observed to be estimated to a linear band of data plots. Nytro 10XN seems to increase exponentially in light emission as the PD magnitude increase above a certain threshold limit, $\approx 1.5nC$. It seems as though Nytro 10XN reaches a point where discharges at the same magnitude emit different amounts of light.

Positive streamers are generally at a larger magnitude than the negative streamers, and more crucial for determining danger of electrical breakdown and detrition on insulation liquids and components. Hence, these results are edifying since it seems that light emission measurements can be utilized to determine PD activity for positive streamers. Nevertheless, more tests are needed in order to study these tendencies and very the data.

5.3 Energy Comparison

The combined data from Figure 4.20 and 4.21 is processed to display the correlation between energy in the streamer vs. light emission. Energy is calculated by multiplying the instantaneous HVAC [kV] during a discharge with the magnitude of the PD [pC]. This information is graphed in Figure 5.1 and 5.2, for negative and positive streamers respectively.

$$e[j] = Q[C] * V[V] \tag{Eq. 30}$$

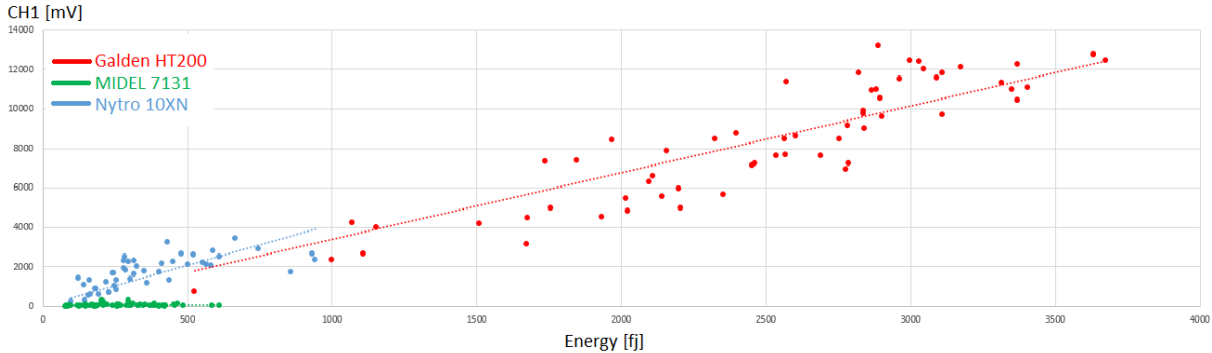


Figure 5.1, PMT light signal vs charge energy (VxQ) for negative PDs.

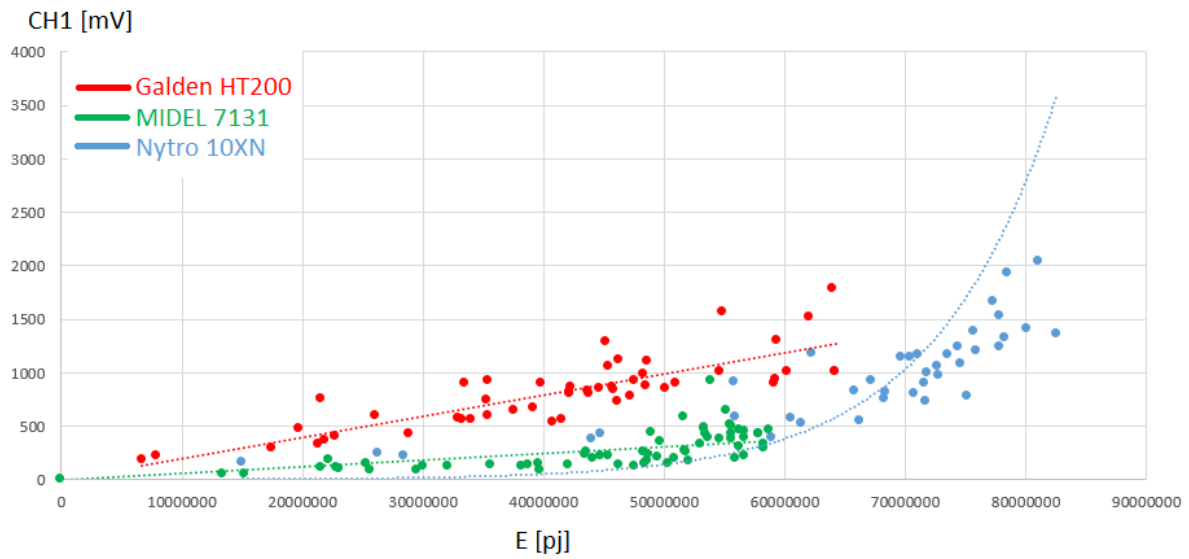


Figure 5.2, PMT light signal vs charge energy (VxQ) for positive PDs.

The general tendencies are quite similar to those observed for PD magnitude and light emission. The negative streamers show a closer correlation between Nytro 10XN and Galden HT200 with respect to energy and light emission, than compared to PD magnitude and light emission. A linear band of data plots seem to fit for these liquids. The negative streamers in MIDEAL 7131 measurements does not seem to contain any direct correlation between light emission and energy, and data points seem more or less arbitrary.

As for the positive streamers, the energy plot is also quite similar to the PD magnitude plot. Compared to Figure 4.21, Figure 5.2 does not stack the great Nytro 10XN PDs on top of each other. There seems to be a tendency for streamers containing high amounts of energy, also emit more light. It is possible to believe that energy in PDs is a more accurate measurement, then just PD magnitude, when observing light emission from PDs. This also have to be studied further.

6. Conclusion

Partial discharges seem to have a correlation between the amount of photon activity and the magnitude of the charge of PDs in dielectric liquids. The correlation is however different for separate dielectric liquids, and may vary greatly. There is also a clear difference in the correlation between negative and positive streamers compared to light emission. Positive streamers show great similarity in light emission and PD activity for different liquids. Further, positive streamers are in general considered more important to understand, than the negative counterparts are. This is due to the positive streamers are of a greater magnitude than the negative, and hence more crucial for the component/insulation condition.

More specifically Nytro 10XN transformer oil, MIDEL 7131 and Galden HT200 all seem to display a clear correlation between large PD activity $>0.5\text{nC}$, and light emission from PDs from positive streamers. Negative streamers are more uncertain, especially for MIDEL 7131.

Registering light emission from PD, and compare it to charge energy seems like a feasible possibility for PD monitoring. The energy have a tendency to be easier to separate than the PD charge magnitude. However, more tests and verified data are needed, before this measurement method can be practically utilized.

The experimental work conducted for this thesis has been successful. Promising and useful tendencies for further work have been discovered and registered. The test setup works sufficiently fine, but has room for improvements, as discussed in the next section.

7. Further Work

The study of comparing light emission and PD is a relative new concept. More collected data is needed for different candidate dielectric liquids. It can be useful to test used transformer oil, in order to achieve near operating scenarios. If an extensive amount of data are collected, light measurement might become a feasible monitoring/detection tool for future power electronic components.

Regarding the experimental work conducted for this thesis, some improvements and further tests are suggested here:

- Test more candidate liquids.
- Vary the HVAC voltage for liquids during tests. This will help collect a broader band of data plots. Electrode distance must be increased in the test cell should this be made possible without electrical breakdown.
- Test the effect of frequency variation.
- Test the effect of pressurised liquids.
- Implement a double PMT setup and a coincidence circuit. This will remove the possibility of measuring dark currents as PD signals.
- Install a different L_r with a wider impedance range. This will help achieve resonance for several frequencies.

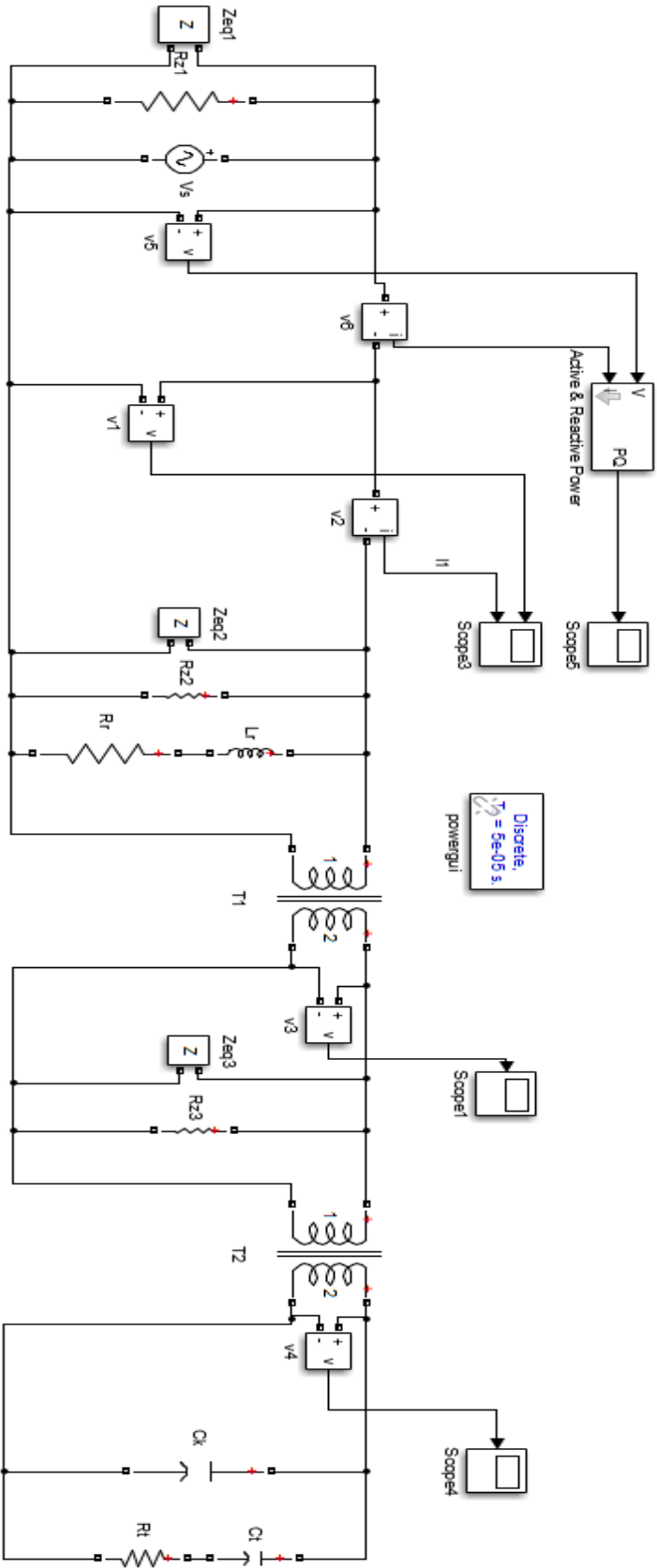
References

- [1] S. E. Research, "PRESSBACK-Pressure Tolerant Power Electronics for Subsea Oil and Gas Exploration," SINTEF, Trondheim, 2013.
- [2] SINTEF, "Power Supply to Subsea Installations," Sintef, Trondheim, 2012.
- [3] R. P. Magnar Hernes, "Enabling pressure tolerant power electronic converters for subsea," SINTEF ENERGY RESEARCH, Trondheim.
- [4] L. E. Lundgaard and S. L. Kyrkjeeide, "Evaluation of Dielectric Liquids by Measurement of Their Partial Discharge Characteristics," pp. 901-909, October 1994.
- [5] E. Kuffel, J. Kuffel and W. Zaengl, High Voltage Engineering Fundamentals, Newnes, 2000.
- [6] E. Ildstad, TET4160 High Voltage Insulation, NTNU, 2012.
- [7] N. Davari, P. O. Åstrand, S. Ingebritsen and M. Unge, "Excitation energies and ionization potentials at high electrical fields for molecules relevant for electrically insulating liquids," *Journal of Applied Physics*, April 2103.
- [8] D. André, "Conduction and breakdown initiation in dielectric liquids," *2011 IEEE International Conference on Dielectric Liquids*, 2011.
- [9] O. Lesaint and P. Gournay, "Evidence of the gaseous nature of positive filamentary streamers in various liquids," *IEEE Annual Report*, pp. 834-839, 1994.
- [10] L. Lundegaard, D. Linhjell and G. Berg, "Propagation of Positive and Negative Streamers in Oil with and without Pressboard Interfaces," *IEEE Transactions on Dielectrics and Electrical Insulation*, June 1998.
- [11] N. Davari, P. O. Åstrand, M. Unge, L. E. L and D. Linhjell, "Field-dependent molecular ionization and excitation energies: Implications for electrically insulating liquids," *AIP*, March 2014.
- [12] R. J. V. Brunt, "Stochastic Properties of Partial Discharge-Phenomena," *IEEE Transactions on Electrical Insulation*, pp. 902-948, October 1991.
- [13] M. v. Laue, "Comment on K. Zuber's Measurement of the Spark Discharge Delay Time," *Ann. Phys. Leipzig*, 1925.
- [14] T. Grav, "Mechanisms Governing the Occurrence of Partial Discharges in Insulation Liquids," June, NTNU, 2013.
- [15] N. Davari, P. O. Åstrand and T. Van Voorhis, "Field-dependent ionisation potential by constrained density functional theory," *Taylor & Francis*, April 2013.

- [16] S. Ingebrigtsen, "The Influence of Chemical Composition on Streamer Initiation and Propagation in Dielectric Liquids," PhD thesis, NTNU, 2008.
- [17] M. Design, M1400/M1400i Owner's Manual, MACKIE: Mackie Design, 2001.
- [18] P. Diagnostix, ICM system, Digital Partial Discharge Recorder, User Manual, 2008.
- [19] HAMAMATSU, PHOTOMULTIPLIER TUBES AND RELATED PRODUCTS, HAMAMATSU PHOTONICS, K.K. : Electron Tube Division, 2010.
- [20] Physical Acoustics Corporation, *PCI-2 BASED AE SYSTEM PCI-2 BASED AE SYSTEM Rev 3*, PHYSICAL ACOUSTICS CORPORATION, 2007.
- [21] Tektronix, Mixed Signal Oscilloscopes MSO5000, DPO5000 Series Datasheet, www.tektronix.com: Tektronix, 2013.
- [22] NYNAS, *Product Data Sheet Nytro 10XN*, NYNAS: reinhardoil.dk, 2012.
- [23] L. Lundegaard, D. Linhjell and G. Berg, "Streamer/Leaders from a Metallic Particle Between Parallel Plane Electrodes in Transformer Oil," *IEEE Transactions on Dielectrics and Electrical Insulation*, December 2001.
- [24] MIDEL, *MIDEL 7131 Dielectric Insulating Fluid Overview*, MIDEL, 2010.
- [25] I. Solvay Solexis, *Galden HT, Heat Transfer Fluid*, Solvay Solexis, 2007.
- [26] ExxonMobile, *Product Safety Summary Exxsol D80*, Exxon Mobile Chemical: Exxon Mobile, 2014.
- [27] "Omicron," Omicron, [Online]. Available: <https://www.omicron.at/en/>. [Accessed 11 2013].
- [28] J. C. Devins, S. J. Rzed and R. J. Schwabe, "Breakdown and prebreakdown phenomena in liquids," *Journal of Applied Physics*, March 1981.
- [29] C. C. Lo and B. Leskovar, "Evaluation of Hamamatsu R1635 photomultiplier," *AIP*, pp. 1100-1103, 12 March 1984.
- [30] Hamamatsu, "Product bulletin PB-103-01," Hamamatsu, 1982.

Appendix A

MATLAB Simulink Model



Appendix B

Transformer tests and calculations

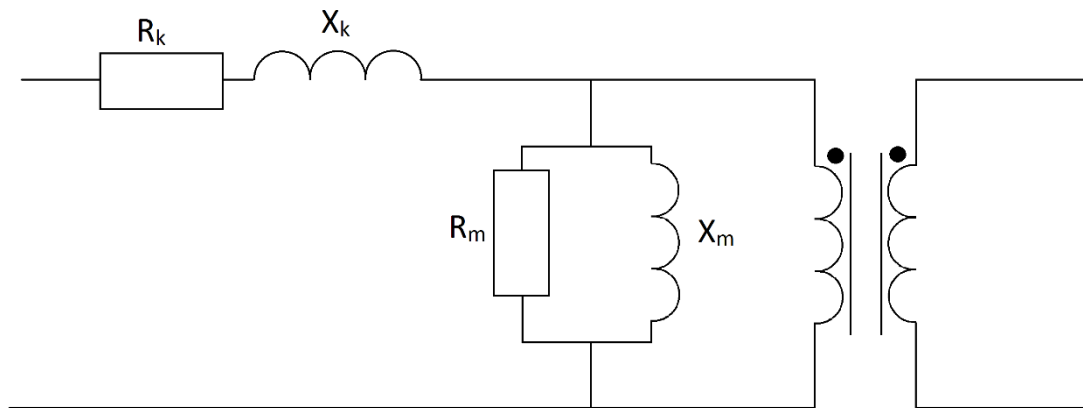


Figure A. 1, Transformer equivalent

Open circuit:

$$R_m = \frac{V^2}{P} \quad A-1$$

$$X_m = \frac{V^2}{Q} \quad A-2$$

$$L_m = \frac{X_m}{2\pi f} \quad A-3$$

Short Circuit:

$$R_k = \frac{P}{I^2} \quad A-4$$

$$X_k = \frac{Q}{I^2} \quad A-5$$

T₂ High Voltage Transformer 220:50 000

F [Hz]	Open Circuit						Short Circuit					
	Voltage [V]	I [A]	P [W]	Q [Var]	S [VA]	PF	Voltage [V]	I [A]	P [W]	Q [Var]	S [VA]	PF
50	20	0.147	0.7	2.9	3	0.18	3.4	8.12	24.8	11.9	27.7	0.9
	50.4	0.392	3.5	19.4	19.7	0.15	4	9.52	34.2	16.3	38	0.9
	100.7	0.797	12.3	79.4	80.3	0.16	3.9	9.33	33.1	15.7	36.8	0.9
	150.3	1.125	27.2	169.9	169.3							
	200.2	1.471	0.2	2	1.7							
100.2	10	0.284	0.5	4.3	4.3	0.11	1	1.99	1.1	1.7	2	0.52
	15.3	0.381	0.8	7.5	7.6		1.6	3.08	2.7	4.2	4.9	
	19.9	0.497	1.2	12.4	12.4	0.1						
	25.1	0.521	2	14.45	14.6							
	28	0.521	2	14.45	14.6	0.14						
200.15	6.1	0.2106	0.1	1.3	1.3		1	1.147	0.4	0.7	1.1	
	10	0.358	0.3	3.5	3.6	0.09	1.6	1.81	0.9	2.7	2.9	
	15.1	0.575	0.8	8.6	8.7		2	2.2	1.3	4.1	4.3	
	20	0.783	1.4	15.6	15.6	0.09	2.4	2.68	1.9	6.2	6.5	0.29
	25	1.002	2.1	24.9	25	0.08	2.8	3.06	2.5	8.1	8.5	0.29
400.7	10.1	0.773	0.9	7.7	7.8	0.12	1	0.668	0.1	0.7	0.7	
	14.9	1.194	2	17.7	17.8	0.11	1.6	1.047	0.3	1.7	1.7	
	20	1.638	3.6	32.5	32.7	0.11	2	1.245	0.4	2.4	2.5	
							2.5	1.56	0.6	3.9	3.9	
							3	1.83	0.8	5.5	5.6	0.15
						3.5	2.08	1	7.1	7.1	0.14	
						4	2.36	1.3	9.2	9.3	0.14	

Hz	Rm	Xm	Xm (test)		Xm average	Lm	Rk	Rk test		Xk
			Xm (test)	Lm				Rk test	Xk	
50	571.428571	136.054422	137.9910345	131.1436646	0.41765498	0.46612903	0.37613143	0.18048242	0.17985135	
	725.76	128.571429	130.9960825	127.7139798	0.45951662	0.46783626	0.37735683	0.1803584	0.17985135	
	824.430081	126.348808	127.7139798	133.6	135.3510485	0.90909091	0.27777076	0.42928209	0.44273908	
	830.518015	500	58.4795322	50	53.76591263	0.94814815	0.28461798	0.42928209	0.44273908	
	468.18	53.8732394	54.43953488	52.2309711	52.80133333	2.5	0.3040417	0.76010426	0.82415067	
100.2	495.0125	50.5030181	50.80725806	53.7428023	54.25605536	2.84444444	0.27471689	0.82415067	0.84710744	
	525.008333	392	28.9648623	28.62307692	26.73031534	3.07692308	0.26859504	0.84710744	0.86322121	
	372.1	27.9929609	28.57142857	26.2608696	26.5127907	3.03157895	0.26453553	0.86322121	0.8650519	
	285.0125	26.2608696	26.5127907	25.5427842	25.64102564	3.136	0.26699133	0.8650519	0.8650519	
	297.619048	24.9500998	25.10040161	13.0659767	13.24805195	10	0.22410269	1.56871885	1.56871885	
200.15	333.333333	27.9929609	28.57142857	26.73031534	0.02126615	8.53333333	0.27367044	1.55079916	1.55079916	
	285.0125	26.2608696	26.5127907	10	0.25806035	10	0.25806035	1.54836212	1.54836212	
	285.714286	25.5427842	25.64102564	10.4166667	0.24654832	11.25	0.23888441	1.64233032	1.64233032	
	297.619048	24.9500998	25.10040161	11.25	0.23113905	12.25	0.23113905	1.64108728	1.64108728	
	113.344444	13.0659767	13.24805195	12.479062	12.54293785	12.3076923	0.23340994	1.65182419	1.65182419	
400.7	111.005	12.479062	12.54293785	12.58501697	0.00500121	10	0.22410269	1.56871885	1.56871885	
	111.11111	12.2100122	12.30769231	8.53333333	0.27367044	10	0.25806035	1.54836212	1.54836212	
				10.4166667	0.24654832	11.25	0.23888441	1.64233032	1.64233032	
				11.25	0.23113905	12.25	0.23113905	1.64108728	1.64108728	
				12.3076923	0.23340994	12.3076923	0.23340994	1.65182419	1.65182419	

T₁ isolating transformer 20/40/60:220

60:220										60:220									
Open Circuit					Short Circuit					Open Circuit					Short Circuit				
f [Hz]	Voltage [V]	I [A]	P [W]	Q [Var]	S [VA]	PF	Voltage [V]	I [A]	P [W]	Q [Var]	S [VA]	PF	f [Hz]	Rm	Xm	Xm average	Lm	Rk	Xk
50	6.5	0.147	0.3	0.9	0.9		0.4	1.494	0.7	0.1	0.7		50	140.833333	46.944444	85.0875181	0.1495046	0.31361501	0.044802145
	10	0.169	0.6	1.6	1.7		1	3.37	3.3	0.5	3.4			166.666667	62.5		0.19904459	0.29057225	0.044026099
	20.1	0.218	1.9	4	4.4		1.5	5.04	7.5	1.2	7.6			212.636842	101.0025		0.32166401	0.29525699	0.047241119
	25.1	0.244	2.8	5.5	6.1		2	6.73	13.4	2.1	13.4			225.003571	114.547273		0.36480023	0.29585211	0.046564883
	39.9	0.412	6.5	15.1	16.5		3	9.81	28.7	4.4	29.2			244.924615	105.431126		0.33576792	0.29822489	0.045720889
45.3	0.595	8.3	25.6	27									247.239759	80.1597656		0.25528588			
100.5	6.5	0.098	0.1	0.6	0.6		0.5	1.743	0.9	0.3	0.9		100	422.5	70.4166667		0.1115706	0.29624275	0.038747584
	10.1	0.118	0.3	1.1	1.2		1	3.22	3.1	0.9	3.2			340.033333	92.7363636		0.1469347	0.29898538	0.086802207
	20	0.163	1.35	2.95	3.2		1.5	4.83	6.9	2.1	7.2			296.296296	135.59322		0.21483838	0.29577048	0.090017103
40	0.223	4.7	7.6	9		2	6.38	12.2	3.6	12.7			340.425532	210.526316		0.33356516	0.2997219	0.088442527	
40:220										40:220									
Open Circuit					Short Circuit					Open Circuit					Short Circuit				
f [Hz]	Voltage [V]	I [A]	P [W]	Q [Var]	S [VA]	PF	Voltage [V]	I [A]	P [W]	Q [Var]	S [VA]	PF	f [Hz]	Rm	Xm	Xm average	Lm	Rk	Xk
50.46	6.5	0.227	0.5	1.4	1.5		0.5	3	1.5	0.3	1.5		50.46	84.5	30.1785714		0.09523395	0.16666667	0.033333333
	10	0.266	1.1	2.4	2.6		1	6.15	6.2	1	6.3			90.9090909	41.666667		0.13148671	0.16392359	0.026439289
	20.4	0.385	3.9	6.9	7.9		1.5	8.87	13.1	2.1	13.2			106.707692	60.3130435		0.19032873	0.16650376	0.026691443
	30.1	0.81	8	23.1	24.5									113.25125	39.2212121		0.12376964		
	40	2.53	14.8	100.4	101.5									108.108108	15.986255		0.05028974		
100.4	6.5	0.182	0.3	1.1	1.2		0.5	2.82	1.3	0.4	1.4		100.4	140.833333	38.4090909		0.0609173	0.16347266	0.05029281
	10	0.219	0.8	2	2.2		1	5.86	5.7	1.7	5.9			125	50		0.07930063	0.16598912	0.049505227
	20.8	0.297	3	5.4	6.1		1.5	8.65	12.4	3.7	13			144.213333	80.1185185		0.12706898	0.16572555	0.049450366
	30.5	0.355	6	9.1	10.9									155.041667	102.225275		0.16213058		
	40	0.43	10	14.1	17.3									160	113.475177		0.1797307		
20:220										20:220									
Open Circuit					Short Circuit					Open Circuit					Short Circuit				
f [Hz]	Voltage [V]	I [A]	P [W]	Q [Var]	S [VA]	PF	Voltage [V]	I [A]	P [W]	Q [Var]	S [VA]	PF	f [Hz]	Rm	Xm	Xm average	Lm	Rk	Xk
50.4	6.5	0.531	1.8	3	3.5		0.5	6.07	2.8	0.4	2.9		50.4	23.4722222	14.0833333		0.04440542	0.07599424	0.010856319
	10.5	0.753	4.3	6.7	8		0.7	8.52	5.7	0.6	5.4			25.6395349	16.4552239		0.05198926	0.07852278	0.008265556
	15.1	1.763	8.5	24.9	26.4		0.8	9.4	7.1	0.8	7.2			26.8247059	9.15702811		0.02893106	0.0803531	0.009053871
	20.4	6.36	18.2	129.2	130.8									22.8659341	3.22106263		0.01017672		
	100.49	6.5	0.419	1.4	2.3	2.7		0.5	5.85	2.6	0.6	2.7		100.49	30.1785714	18.3695652		0.02910827	0.07597341
10.3	0.516	3.1	4.3	5.3	5.3		0.7	8.47	5.6	1.2	5.7			34.2225806	24.672093		0.03990521	0.07805868	0.01672686
15.2	0.655	6.3	7.7	10	10		0.8	9.31	6.8	1.4	7			36.6730159	30.0051948		0.047546	0.078453	0.016152088
20	0.813	10.4	12.4	16.2	16.2									38.4615385	32.2580645		0.05111588		

Appendix C

Small negative PD data.

Nytro 10XN				MIDEL7131				Galden			
CH1, LYS [mv]	CH2,ICM[pC]	CH3,HV,V		CH1, LYS [mV]	CH2,ICM[mv]	CH3,HV,V		CH1, LYS [mv]	CH2,ICM[mv]	CH3,HV,V	
2044	15,9	36,54	580,986	60	8,28	22,32	184,8096	7880	78,8	27,36	2155,968
2296	7,8	35,82	279,396	79,8	11,2	19,8	221,76	11520	107,6	27,54	2963,304
2324	8,6	36,54	314,244	46,2	21,6	22,5	486	4520	72	26,82	1931,04
2646	13,2	36,36	479,952	56	5,92	21,6	127,872	10960	106	27,18	2881,08
2604	16,5	31,5	519,75	79,8	7,68	22,14	170,0352	7240	103,2	27	2786,4
1218	6,3	34,56	217,728	40,6	10,88	22,14	240,8832	11800	102,4	27,54	2820,096
2268	9	32,94	296,46	22,4	5,76	21,78	125,4528	10440	123,2	27,36	3370,752
602	5,4	35,82	193,428	40,6	18,08	22,32	403,5456	8480	91,6	25,38	2324,808
1330	5,4	29,98	161,892	28	3,68	21,96	80,8128	11360	95,2	27	2570,4
602	4,7	34,92	164,124	228,2	9,44	22,14	209,0016	4840	76	26,62	2023,12
2534	10,7	26,46	283,122	96,6	16	22,14	354,24	7640	101,6	26,46	2688,336
2800	17,1	34,38	587,898	18,2	19,04	22,14	421,5456	11320	121,2	27,36	3316,032
1190	9,9	36,54	361,746	22,4	6,88	21,78	149,8464	12240	123,2	27,36	3370,752
3248	11,7	36,72	429,624	165,2	13,44	22,32	299,9808	7640	97,2	26,1	2536,92
252	4,6	21,42	98,532	0	8,8	20,34	178,992	7320	65,2	26,64	1736,928
1652	6,9	35,1	242,19	75,2	12	21,42	257,04	12400	110	27,54	3029,4
1694	6,8	36	244,8	40,6	4,16	22,14	92,1024	10920	107,6	26,64	2866,464
2212	15,3	36,18	553,554	23,8	3,84	22,14	85,0176	9600	106	27,36	2900,16
2114	15,9	35,64	566,676	30,8	26,88	21,78	585,4464	5560	78,8	27,18	2141,784
1022	6,8	36,36	247,248	95,2	20,64	21,96	453,2544	11560	114,4	27	3088,8
672	6,3	36,36	229,068	30,8	5,76	20,88	120,2688	12000	112	27,18	3044,16
2142	12,2	33,66	410,652	44,8	18,08	21,6	390,528	7240	90	27,36	2462,4
1064	5,4	26,28	141,912	26,6	12,16	22,14	269,2224	5480	73,2	27,54	2015,928
2534	17,1	35,64	609,444	70	13,92	21,96	305,6832	7680	96,4	26,64	2568,096
1708	11,1	36,36	403,596	51,8	18,72	22,14	414,4608	8760	94,4	25,38	2395,872
1834	7,8	36,9	287,82	37,8	14,72	22,32	328,5504	12760	132,8	27,36	3633,408
868	5,1	35,82	182,682	26,6	18,88	22,32	421,4016	7120	89,6	27,36	2451,456
882	4,9	37,08	181,692	28	16,64	22,32	371,4048	11080	124,4	27,36	3403,584
1642	9,3	34,02	316,386	51,8	19,36	21,96	425,1456	9160	102,4	27,18	2783,232
2016	11,1	29,16	323,676	35	15,88	21,96	348,7248	6600	77,6	27,18	2109,168
546	4,2	37,44	157,248	44,8	13,76	21,78	299,6928	4480	61,6	27,18	1674,288
1316	6,8	37,62	255,816	50,4	20,64	22,14	456,9696	12120	117,6	27	3175,2
3430	17,9	37,08	663,732	53,2	9,44	22,14	209,0016	8480	97,6	26,28	2564,928
2366	24,7	38,16	942,552	18,2	17,92	22,5	403,2	10560	107,2	27	2894,4
1386	11,3	26,64	301,032	16,8	4	22,14	88,56	12480	109,6	27,36	2998,656
2240	12,2	36,9	450,18	159,6	21,28	21,96	467,3088	4960	66,8	26,28	1755,504
1722	24,6	34,92	859,032	217	9,12	22,14	201,9168	6960	100,8	27,54	2776,032
2926	19,8	37,62	744,876	98	6,72	22,32	149,9904	6320	79,2	26,46	2095,632
1330	11,6	37,62	436,392	84	15,68	21,6	338,688	13200	108,4	26,64	2887,776
1428	3,2	37,98	121,536	0	8,32	22,14	184,2048	8460	102	27	2754
294	3,9	37,08	144,612	56	6,88	20,88	143,6544	9920	104,4	27,18	2837,592
2674	24,6	37,8	929,88	28	7,84	21,06	165,1104	8640	98,4	26,46	2603,664
1778	9,5	36,9	350,55	142,8	17,76	21,78	386,8128	5640	86	27,36	2352,96
812	6,7	37,8	253,26	26,6	7,36	20,7	152,352	5960	82	26,82	2199,24
700	6,2	36,72	227,664	43,4	13,44	21,6	290,304	3160	62,4	26,82	1673,568
2128	13,3	37,8	502,74	0	11,68	22,14	258,5952	8400	72,4	27,18	1967,832
1904	10,1	27,72	279,972	65,8	28,48	21,42	610,0416	11800	115,2	27	3110,4
				270	9,12	22,14	201,9168	4960	82,8	26,64	2205,792
				18,2	11,52	22,32	257,1264	12440	135,2	27,18	3674,736
				95,2	12,48	21,06	262,8288	9760	104,4	27,18	2837,592
				23,8	8,48	22,32	189,2736	11000	122,4	27,36	3348,864
				36,4	15,84	20,88	330,7392	9000	105,2	27	2840,4
				63	8,64	20,88	180,4032	9720	116	26,82	3111,12
				126	14,08	22,14	311,7312	4000	50,4	22,86	1152,144
				9,8	4	19,8	79,2	760	20,8	25,2	524,16
				57,4	17,28	21,96	379,4688	2360	39,6	25,2	997,92
				47,6	15,36	21,6	331,776	2680	45,2	24,48	1106,496
				47,6	12	22,14	265,68	4200	60,8	24,84	1510,272
				58,8	4,96	19,8	98,208	4240	42,4	25,2	1068,48
				277,2	13,28	22,32	296,4096	7400	73,2	25,2	1844,64

Large positive PD data.

Nytro 10XN				MIDEL7131				Galden			
CH1, LYS [mv]	CH2,ICM[pC]	CH3,HV,V		CH1, LYS [mV]	CH2,ICM[mv]	CH3,HV,V		CH1, LYS [mv]	CH2,ICM[mv]	CH3,HV,V	
1668	2064	37440	77276160	126	1238,4	25920	32099328	672	1056	37080	39156480
1356	2076	39780	82583280	230	1828,8	26640	48719232	860	1150,6	36772	42309863,2
1536	2088	37260	77798880	446	2044,8	27720	56681856	740	970,2	36360	35276472
756	1896	36000	68256000	122	1713,6	27720	47500992	432	778,8	37080	28877904
1380	2052	36900	75718800	466	2116,8	27720	58677696	868	1221	37440	45714240
384	1272	34600	44011200	176	1814,4	26820	48662208	1008	1663,2	36180	60174576
1320	2112	37080	78312960	146	1756,8	27540	48382272	600	730,4	35640	26031456
492	1560	34200	53352000	424	2044,8	27180	55577664	822	1179,2	37080	43724736
1200	2088	36360	75919680	94	1152	25560	29445120	876	1302,4	37260	48527424
996	2016	35640	71850240	440	1915,2	25560	48952512	852	1372,8	36540	50162112
912	1812	30780	55773360	432	1929,6	27720	53488512	924	1302,4	36540	47589696
900	2040	35100	71604000	126	1209,6	24840	30046464	222	264	29980	7914720
1164	2004	35460	71061840	298	2102,4	27720	58278528	576	932,8	35280	32909184
1140	2028	34740	70452720	140	1569,6	24660	38706336	900	1381,6	36900	50981040
1404	2088	38340	80053920	276	1929,6	26820	51751872	372	642,4	34020	21854448
2040	2076	39060	81088560	482	2001,6	26640	53322624	564	950,4	35820	34043328
1932	2028	38700	78483600	194	1857,6	27360	50823936	900	1601,6	36900	59099040
1236	2088	37260	77798880	202	1713,6	25740	44108064	930	959,2	36900	35394480
1176	1800	34560	62208000	326	1900,8	27900	53032320	1122	1240,8	37260	46232208
828	1956	33660	65838960	252	1814,4	26640	48335616	336	633,6	33660	21326976
1140	1944	35820	69634080	264	2001,6	25920	51881472	642	1038,4	36180	37569312
1236	2076	35820	74362320	138	1526,4	27540	42037056	990	1302,4	37080	48292992
1080	2052	36360	74610720	388	1972,8	27180	53620704	906	915,2	36540	33441408
1164	2052	35820	73502640	48	748,8	20340	15230592	474	572	34560	19768320
816	2052	33300	68331600	204	1843,2	26820	49434624	750	616	34920	21510720
780	2076	36180	75109680	302	2030,4	27720	56282688	294	510,4	34200	17455680
732	2064	34740	71703360	150	1526,4	25920	39564288	1302	1601,6	37080	59387328
156	516	29160	15046560	216	2044,8	27720	56681856	1520	1689,6	36720	62042112
432	1464	30600	44798400	92	1137,6	22500	25596000	816	1170,4	36000	42134400
972	2052	35460	72763920	466	2016	27900	56246400	400	660	34380	22690800
396	1788	32940	58896720	228	1843,2	23580	43462656	560	906,4	36720	33283008
1056	2040	35640	72705600	334	2102,4	27720	58278528	896	1135,2	35100	39845520
576	1980	30600	60588000	430	2088	27720	57879360	1288	1267,2	35640	45163008
528	1884	32580	61380720	358	1814,4	27360	49641984	1008	1487,2	36720	54609984
924	1956	34380	67247280	132	1382,4	25740	35582976	1784	1733,6	36900	63969840
804	2004	35280	70701120	86	1440	27540	39657600	1056	1223,2	37080	45356256
552	1908	34740	66283920	152	1828,8	27540	50365152	184	237,6	28260	6714576
240	1020	25740	26254800	512	2001,6	27720	55484352	592	959,2	36900	35394480
216	1032	27540	28421280	380	1972,8	27720	54686016	736	1276	36180	46165680
588	1716	32580	55907280	424	2088	27720	57879360	1010	1749	36720	64223280
1008	1800	35640	64152000	176	1900,8	27360	52005888	800	1133	37260	42215580
				384	2030,4	27360	55551744	840	1287	35640	45868680
				136	1670,4	27720	46303488	560	1166	35640	41556240
				0	0	0	0	540	1144	35640	40772160
				112	1008	21420	21591360	850	1221	36540	44615340
				224	1728	26280	45411840	800	1221	35820	43736220
				128	1483,2	25740	38177568	940	1639	36180	59299020
				392	2059,2	27540	56710368	1570	1485	36900	54796500
				196	2016	27720	55883520	1110	1331	36540	48634740
				104	1022,4	22500	23004000	780	1287	36720	47258640
				108	1022,4	22320	22819968				
				924	1929,6	27900	53835840				
				640	2001,6	27540	55124064				
				584	1886,4	27360	51611904				
				148	1108,8	22860	25347168				
				184	1108,8	19980	22153824				
				220	1800	24840	44712000				
				260	1656	26280	43519680				
				504	2044,8	27180	55577664				
				56	604,8	22140	13390272				